

## Angular-gain spectrum of free-electron lasers

W. B. Colson

Berkeley Research Associates, P.O. Box 241, Berkeley, California 94701

G. Dattoli and F. Ciocci

ENEA Div., Laser di Potenza, Caixa Postale 65, 00044 Frascati, Roma, Italy

(Received 7 June 1984)

The theory of free-electron lasers is extended to include the new coupling between an electron beam and optical wave propagating at an angle  $\vartheta$  in an arbitrary harmonic. The coupling allows the laser to be tuned to a wider range of wavelengths and to include the effects of emittance in the electron beam. The formulation of the results in terms of coupling constants means that the existing knowledge of high gain, low gain, weak optical fields, strong optical fields, and short pulses in free-electron lasers can be immediately generalized to off-axis propagation in an arbitrary harmonic.

### I. INTRODUCTION

In a free-electron laser (FEL) oscillator, a beam of relativistic electrons is injected into an undulator magnet where they undergo transverse oscillations. The undulating electrons couple to and amplify co-propagating laser light which may be stored in an optical resonator. There is significant research exploring both the experimental and theoretical aspects of FEL operation in the range from millimeter to x-ray wavelengths.<sup>1-9</sup>

One of FEL's most attractive features is its ability to produce tunable radiation. This is usually accomplished by changing the initial electron beam energy,  $\gamma mc^2$ , but it has been shown that the range of tunability may be further extended to shorter wavelengths by exploiting odd-numbered higher harmonics on axis in a linearly polarized undulator.<sup>10-15</sup> Gain off axis at the fundamental wavelength has been calculated for the case of a weak electromagnetic undulator field.<sup>16,17</sup> The electromagnetic undulator can be related to the magnetic undulator using the Weizsäcker-Williams approximation.<sup>18,19</sup>

In this paper, we calculate the FEL gain at all angles in both the helical and the linearly polarized undulators in all higher harmonics. Shown in Fig. 1 is an FEL oscillator schematic with the optical mode skewed at angle  $\vartheta$  with respect to the electron beam and undulator axis. Relativistic electrons with longitudinal velocity  $\beta_z c$  travel along the magnetic undulator and oscillate in the transverse direction with frequency  $\beta_z \omega_u$ , where  $\omega_u = 2\pi c / \lambda_u$ ,  $\lambda_u$  is the undulator wavelength, and  $c$  is the speed of light. In weak undulator fields  $\beta_z \approx 1 - 1/2\gamma^2$ , and the resulting emission frequency received at an angle  $\vartheta$  is centered at<sup>20,21</sup>

$$\omega^* = \frac{\beta_z \omega_u n}{1 - \beta_z \cos \vartheta} \approx \frac{2\gamma^2 \omega_u n}{1 + \gamma^2 \vartheta^2},$$

where  $n$  labels the harmonic ( $n = 1$  denotes the fundamental). Since the emission is predominantly confined to a forward cone with  $\vartheta < \gamma^{-1}$ , a small angle expansion is used when  $\gamma \gg 1$ . The large factor  $\gamma^2$  shows how the

FEL makes use of a large Doppler shift to emit at frequencies much higher than the electron oscillation frequency  $\beta_z \omega_u$ . A typical undulator wavelength is  $\lambda_u \approx 3$  cm so that  $\gamma \approx 200$  gives optical frequencies in the fundamental  $n = 1$ . If the eleventh harmonic is used, then only  $\gamma = 60$  is needed to reach the same wavelength. In any wavelength range, a change in the angle  $\vartheta$  can be used to tune the FEL frequency with  $n, \lambda_u$ , and  $\gamma$  fixed. If  $\gamma \vartheta \approx 1$ , the emission frequency is decreased by half. Sometimes experiments with  $\gamma \gg 1$  are not sufficiently aligned, nor is the electron beam of sufficient angular quality (nonzero emittance) to allow all electrons to radiate coherently at the expected frequency. In that case, the coupling calculated in this paper can help diagnose the operation of an FEL.

In Sec. II we derive the perfect trajectories of an electron in a helical undulator and present the resulting spontaneous emission spectrum  $d^2I(\omega, \vartheta)/d\Omega d\omega$ . Also in Sec. II the FEL gain surface  $G(\omega, \vartheta)$  is calculated for the helical undulator. In Sec. III, we discuss the same results for a linearly polarized undulator. In Sec. IV, an expression is calculated for the net gain from an electron beam with nonzero emittance. Finally, in Sec. V there is a discussion with some remarks on the Madey theorem.<sup>22</sup>

### II. SPONTANEOUS EMISSION FROM PERFECT HELICAL TRAJECTORIES

The emission spectrum from any electron is determined by its trajectory, or path through the undulator. Unlike

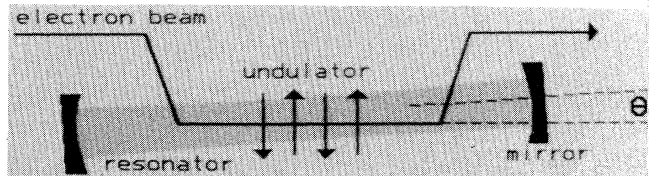


FIG. 1. FEL schematic shows an electron beam propagating through a periodic undulator, but with the optical resonator tilted at an angle  $\vartheta$ .

the broadband synchrotron radiation from a relativistic electron in a bending magnet,<sup>23</sup> the FEL undulator radiation can have a spectrum rich with detailed structure<sup>24</sup> in frequency  $\omega$  and emission angle  $\vartheta$ . The same physical principles give the detailed structure to the FEL gain spectrum that will be calculated later.

The electron trajectories are determined by the Lorentz force equations of motion

$$\frac{d\vec{\beta}_T}{dt} = -\frac{e}{\gamma mc}(\vec{\beta} \times \vec{B})_T, \quad \frac{d\gamma}{dt} = 0, \quad \gamma^{-2} = 1 - \beta_z^2 - \beta_T^2, \quad (2.1)$$

where  $\vec{\beta}c$  is the electron velocity,  $\vec{\beta}_T c = (\beta_x c, \beta_y c, 0)$  is the transverse electron velocity,  $\vec{B}$  is the undulator field,  $m$  is the electron mass, and  $e = |e|$  is the electron charge magnitude. We ignore the longitudinal equation of motion because its first integral is already known from the Lorentz factor  $\gamma$ , so that (2.1) completely specifies the general motion. The magnetic field of the helical undulator is

$$\vec{B}_h = (B \cos(k_u z), B \sin(k_u z), 0) \quad \text{for } 0 < z < L, \quad (2.2)$$

where  $B$  is the peak field strength,  $\lambda_u = 2\pi/k_u$  is the undulator wavelength, and  $L = N\lambda_u$  is the undulator length. This representation is only accurate if the electron's path remains near the undulator axis where there are no betatron oscillations.<sup>25,26</sup> With perfect injection into helical orbits the first integral of the motion is exactly

$$\frac{d^2 I}{d\Omega d\omega} = \frac{8(e\gamma N)^2}{c} \sum_{n=1}^{\infty} \left[ \frac{n\xi}{K} \frac{\sin(\nu_n)}{\nu_n} \right]^2 \left[ J_{n+1}^2(n\chi) + J_{n-1}^2(n\chi) - \frac{2(1+K^2)}{K^2} J_n^2(n\chi) \right], \quad (2.5)$$

where  $J_n$  is the  $n$ th order Bessel function of the first kind, and

$$\chi = \frac{2K\gamma\vartheta}{1+K^2+\gamma^2\vartheta^2}, \quad 2\xi = \frac{K^2}{1+K^2+\gamma^2\vartheta^2}, \quad \nu_n = \left[ n - \frac{\omega}{2\gamma^2\omega_u} (1+K^2+\gamma^2\vartheta^2) \right] N\pi.$$

The spectral width of each emission line is determined by the number of periods  $N$  in the argument of  $\sin^2(\nu_n)/\nu_n^2$ . Emission occurs in a narrow range of wavelengths satisfying  $\nu_n \approx 0$ . The resonant frequency  $\omega^*$  satisfies  $\nu_n = 0$ . The existence of energy spread or emittance in the electron beam will cause inhomogeneous broadening of the line.<sup>32</sup>

The properties of the emitted radiation as expressed in (2.5) depend crucially on the size of the parameter  $K$ . For  $K < 1$ , only small harmonic numbers contribute to the emission. For  $K \sim 1$ , the energy in the fundamental increases, and the first few harmonics also have comparable intensity. For  $K > 1$ , more harmonics appear. Finally for  $K \gg 1$ , there are many closely spaced harmonics, and the emission spectrum is close to the broadband synchrotron spectrum of a bending magnet.<sup>23</sup> For  $K < 1$ , the magnet is called an "undulator," while for  $K \gg 1$  it is called a

$$\vec{\beta}_T = \left[ -\frac{K}{\gamma} \cos(k_u z), -\frac{K}{\gamma} \sin(k_u z), 0 \right], \quad (2.3)$$

where  $K = e\bar{B}\lambda_u/2\pi mc^2$  and  $\bar{B} = B$  is the root-mean-square magnetic field for the helical undulator. We will see that  $K$  is an important parameter determining the characteristics of spontaneous emission and gain spectra in higher harmonics. The last equation in (2.1) gives  $\gamma^{-2}(1+K^2) = 1 - \beta_z^2$ . Integrating further with constants of integration set equal to zero (perfect injection), the exact trajectory is

$$\vec{r}(t) = \left[ -\frac{K\lambda_u}{2\pi\gamma} \sin(\beta_z \omega_u t), \frac{K\lambda_u}{2\pi\gamma} \cos(\beta_z \omega_u t), \beta_z ct \right]. \quad (2.4)$$

In a typical FEL  $\lambda_u = 3$  cm,  $N = 10^2$ ,  $\gamma = 10^2$ , and  $K = 1$  so that the electrons travel at speed  $\approx c$  along the  $z$  axis for several meters while executing small transverse oscillations with amplitude  $K\lambda_u/2\pi\gamma \approx 50$   $\mu\text{m}$ .

The transverse deflections cause radiation in the forward direction. The characteristics of the spontaneous emission spectrum from an electron in a helical trajectory has been discussed in a number of previous papers,<sup>11,20,27-32</sup> but we review the work again to better clarify the calculation of off-axis gain in the next section. The energy emitted into a frequency interval  $d\omega$  and a solid angle  $d\Omega$  is calculated by means of the Lienard-Wiechert potential in a straightforward way.<sup>20,21</sup> It has been shown that for a large number of undulator periods  $N \gg 1$ , the radiation must become azimuthally symmetric;<sup>31</sup> this fact simplifies the derivation. For  $\gamma \gg 1$  we can expand the small emission angle  $\vartheta$  and write the intensity distribution as

"wiggler."<sup>29,30</sup>

Figure 2 plots the radiated intensity distribution  $d^2 I/d\Omega d\omega$  for the helical undulator with  $K = 0.5$  as a function of  $\gamma\vartheta$  and the dimensionless frequency  $\omega/2\gamma^2\omega_u$ . Figure 2 actually plots intensity with brighter points (white) in the  $(\gamma\vartheta, \omega/2\gamma^2\omega_u)$  plane indicating peak emission of  $[8(e\gamma N)^2/c] \times 0.04$ , while black areas indicated no emission. The scale at the top can be used to evaluate the intermediate grey emission intensities. Only the narrow regions satisfying  $\nu_n \approx 0$  show significant amounts of radiation. We have plotted (2.5) for a relatively short undulator with  $N = 5$  in order to make the emission more visible; typically,  $N = 100$ , and the lines are much more narrow. The fractional linewidth is given by  $|\nu_n| < \pi$ , or  $\delta\omega/\omega^* < 1/2N$ . The frequency at the line center of each harmonic is shifted towards lower frequencies with increasing  $\vartheta$  according to the relationship

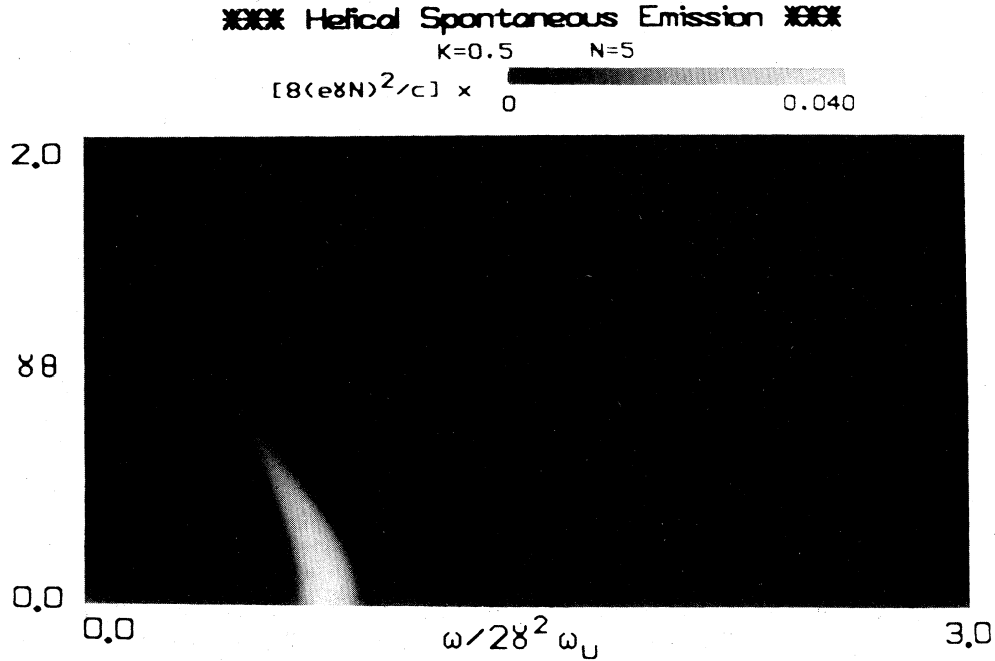


FIG. 2. FEL spontaneous emission intensity from a helical undulator is plotted as a function of  $\gamma\vartheta$  and frequency  $\omega/2\gamma^2\omega_u$  for  $K=0.5$  and  $N=5$ . The intensity scale is indicated in grey  $\times [8(e\gamma N)^2/c]$ . Only the fundamental shows emission at this small value of  $K$ .

$$\omega^* = \frac{2\gamma^2\omega_u n}{1 + K^2 + \gamma^2\vartheta^2} \quad (2.6)$$

On axis only the first harmonic contributes, but for  $\vartheta > 0$  other harmonics may be present. When  $K$  is small ( $K=0.5$  in Fig. 2), only the first harmonic has appreci-

able intensity compared to the intensity in higher harmonics.

Figure 3 shows the same plot as Fig. 2, but with  $K=1.0$ . The grey scale at the top indicates peak emission of  $[8(e\gamma N)^2/c] \times 0.063$ . Increasing  $K$  from 0.5 to 1.0 increases the contribution of the harmonics off axis. There

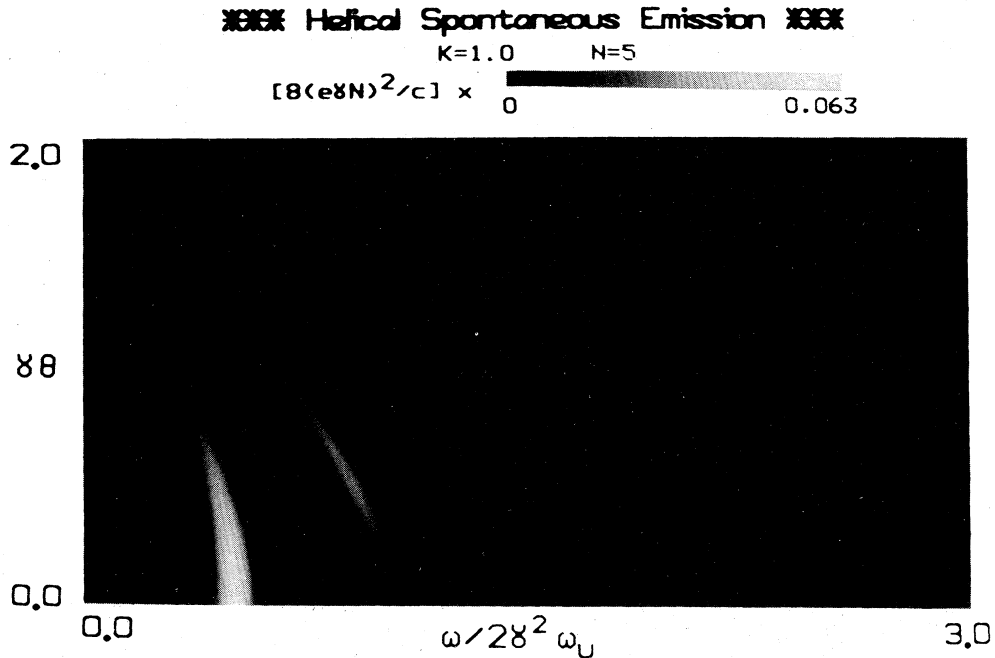


FIG. 3. FEL spontaneous emission intensity from a helical undulator is plotted for  $K=1.0$  and  $N=5$ . Due to the higher value of  $K$ , there is more emission in the higher harmonics off axis and the emission frequency at each harmonic is lower with increasing  $K$  and  $\gamma\vartheta$ .

is still no emission on axis except in the fundamental for the helical undulator. The line centers at  $\omega^*$  decrease with angle  $\vartheta$  according to (2.6), but keep the same fractional width.

To better illustrate the angular dependence Fig. 4 plots the intensity at the line center  $\omega^*$  for the first eight harmonics as a function of  $\gamma\vartheta$  with  $K=1$ . Off axis the peak emission is near  $\gamma\vartheta \approx 1$ , and moves farther off axis in higher harmonics. The intensity is again plotted in units of  $[8(e\gamma N)^2/c]$ .

Figure 5 shows the intensity of the line center  $\omega^*$  versus  $K$  at  $\gamma\vartheta=1$  in the first six harmonics. For all the harmonics at this characteristic angle, the peak emission is near  $K \approx \sqrt{2}$ . While the power in each lower harmonic first increases then decreases with  $K$ , the total power increases with  $K$ , and the spectrum starts to become broad with contributions from many harmonics.

#### A. Imperfect helical trajectories

When electrons enter the undulator with imperfect initial conditions, they will deviate from the ideal helical orbits. There will then be oscillations in the resonance condition with respect to a co-propagating light wave. The more complex motion caused by the imperfect injection reduces the coupling to the optical fundamental frequency, and also causes emission and gain in higher harmonics. For slight angles, a misaligned electron beam is equivalent to a slightly misaligned light wave.

We integrate the equations of motion (2.1) in the helical field (2.2), but now with a constant of motion  $\vartheta = \beta_x(0)/\beta_z(0)$  describing the imperfect injection angle. The resulting paths are not perfect helices as in (2.3). Now we have

$$\vec{\beta}_T = \left[ -\frac{K}{\gamma} \cos(k_u z) + \vartheta, -\frac{K}{\gamma} \sin(k_u z), 0 \right]. \quad (2.7)$$

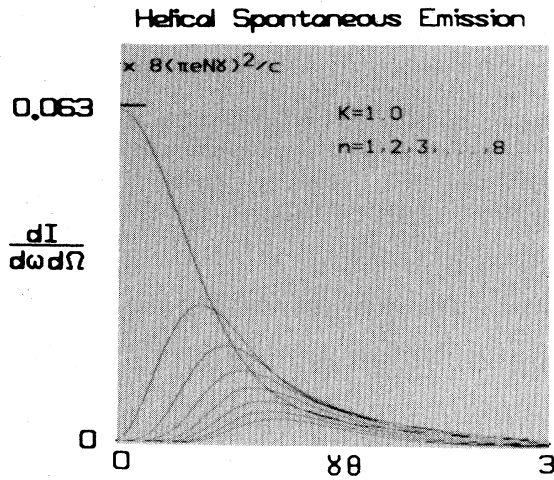


FIG. 4. The peak FEL spontaneous emission intensity from a helical undulator is plotted as a function of  $\gamma\vartheta$  in the first eight harmonics for  $K=1.0$ . Only the fundamental has emission on axis at  $\vartheta=0$ . As the harmonic number increases, the peak intensity decreases and moves to a larger value of  $\gamma\vartheta$ .

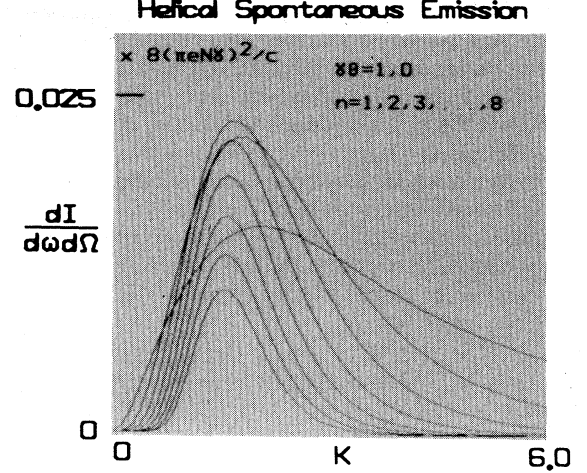


FIG. 5. The peak FEL spontaneous emission intensity from a helical undulator is plotted as a function of  $K$  in the first eight harmonics for  $\gamma\vartheta=1.0$ . As the harmonic number increases, the peak intensity first increases, then decreases, and moves to smaller values of  $K$ . The fundamental,  $n=1$ , is broader in  $K$ , while the higher harmonics are progressively more narrow.

The constant  $\vartheta$  leads to a drifting of the electron beam in the  $x$  direction. For a long helical undulator, it is clear that a drift in  $x$  is equivalent to a drift in  $y$  so we neglect the  $y$  component constant of integration without loss of generality. The effect of this drift is accumulated over the undulator length  $L = N\lambda_u$ . The slow drift alone can be obtained by averaging (2.7) over an integral number of undulator periods to get  $\bar{r}_T = \vartheta ct = \vartheta L \tau$ , where  $\tau = ct/L$ . Note that  $\tau=0 \rightarrow 1$  when an electron passes through the undulator. Typically  $L \approx 3$  m, and  $\vartheta \approx 10^{-3}$  so that  $\bar{r}_T$  at  $\tau=1$  gives a deflection in the transverse direction of about 0.3 mm.

The transverse motion is directly coupled to the longitudinal motion  $z(t)$  because the electron energy is constant. So

$$\beta_z^2 = 1 - \frac{1+K^2}{\gamma^2} + \frac{2K\vartheta}{\gamma} \cos(k_u z) - \vartheta^2. \quad (2.8)$$

Averaging over one or a number of undulator periods breaks up the motion into "fast oscillating" terms and "slow-drift" terms. The slow-drift terms are

$$\bar{\beta}_z = 1 - \frac{1+K^2}{2\gamma^2} - \frac{\vartheta^2}{2}, \quad \bar{z} = \bar{\beta}_z ct, \quad (2.9)$$

where we have assumed  $\gamma \gg 1$  and  $\vartheta \ll 1$ . The fast motion is

$$\Delta\beta_z(t) = \frac{K\vartheta}{\gamma} \cos(\omega_u t), \quad \Delta z(t) = \frac{K\vartheta\lambda_u}{2\pi\gamma} \sin(\omega_u t). \quad (2.10)$$

We have used  $\bar{\beta}_z \approx 1$  to simplify the argument of the fast oscillating terms. The exact solution involves integrals over elliptic integrals, and small oscillations within the arguments of the oscillating terms of (2.10), but since the coefficients  $K\vartheta/\gamma$  are already small, these extra oscillations

tions have been shown to be inconsequential in the results that follow.<sup>11</sup> The fast oscillations (2.10) accurately express the physics that we need to address in this calculation. These  $z$  oscillations cause emission into higher harmonics and reduce the coupling to the electromagnetic wave when  $\vartheta > 0$ .

Before actually calculating the new coupling, we can estimate when the fast  $z$  motion becomes important. Since bunching on the optical wavelength scale is the key to any coherent emission process, the fast  $z$  motion becomes important when its amplitude is comparable to  $\lambda$ . Consider the oscillating phase

$$k\Delta z \approx \frac{K\vartheta k\lambda_u}{2\pi\gamma} \sin(\omega_u t) \approx \frac{2K\gamma\vartheta}{(1+K^2+\gamma^2\vartheta^2)} \sin(\omega_u t), \quad (2.11)$$

where  $k = 2\pi/\lambda = 2\pi c/\omega$ . When  $\gamma\vartheta$  and  $K$  are comparable to unity, the amplitude of  $k\Delta z$  is large enough to cause emission and gain into higher harmonics and reduce the coupling to the fundamental.

#### B. The pendulum equation with imperfect helical trajectories

To calculate the off-axis coupling, we add an optical field to the equation of motion (2.1). The calculational technique is similar to that exploited earlier to evaluate the gain in higher FEL harmonics on axis.<sup>11,13</sup> The optical vector potential is

$$\vec{A}_n = \frac{E}{nk_1} [\sin(\psi), \cos(\psi), 0], \quad (2.12)$$

where  $\psi = nk_1 z - n\omega_1 t + \varphi$ , the carrier frequency in the fundamental is  $\omega_1 = k_1 c$ , the carrier frequency is  $\omega = nck_1$ , and the harmonic number is  $n = 1, 2, 3, \dots$ . This form of  $\vec{A}_n$  explicitly displays the dependence on the harmonic number  $n$ , and will simplify our results to the same form as those already known for the fundamental.  $\vec{A}_n$  is taken to have a slowly varying amplitude  $E$  and phase  $\varphi$ . Neglecting the small transverse optical force<sup>33</sup> when  $\gamma \gg 1$ , in the Lorentz force equation, the transverse motion is solved immediately and the result is the same as (2.7).

Substitution of  $\vec{\beta}_T$  into the fourth component of the Lorentz equation gives

$$\frac{d\gamma}{dt} = \frac{e}{mc^2} \frac{\partial \vec{A}}{\partial t} \cdot \vec{\beta}_T = \frac{eE}{mc} \left[ \frac{K}{\gamma} \cos(k_u z + \psi) + \vartheta \cos(\psi) \right]. \quad (2.13)$$

The two terms on the right oscillate at quite different frequencies. The argument  $(k_u z + \psi)$  evolves slowly when the FEL is near resonance, while  $\psi$  evolves  $\approx \gamma^2$  times faster. When (2.13) is averaged over a discrete number of undulator periods, the fast oscillating term become very small or even zero. The important phase evolution is  $(k_u z + \psi)$  which can be written in a more convenient and sufficiently accurate form:

$$\begin{aligned} k_u z + \psi &= (nk_1 + k_u)z - n\omega_1 t + \varphi \\ &= n(k_1 + k_u)z - n\omega_1 t - (n-1)k_u z + \varphi \\ &\approx n\bar{\xi} + \varphi - (n-1)\omega_u t + n\chi \sin(\omega_u t) - n\Delta v\tau, \end{aligned} \quad (2.14)$$

where

$$\begin{aligned} \bar{\xi} &= (k_1 + k_u)z - \omega_1 t, \\ \chi &= K\vartheta k_1 \lambda_u / 2\pi\gamma \\ &\approx 2K\gamma\vartheta / (1 + K^2 + \gamma^2\vartheta^2), \end{aligned}$$

and

$$\Delta v = 2\pi N\gamma^2\vartheta^2 / (1 + K^2 + \gamma^2\vartheta^2).$$

Then (2.13) becomes

$$\frac{d\gamma}{dt} = \frac{eKE}{\gamma mc} \cos[n\bar{\xi} + \varphi - n\Delta v\tau - (n-1)\omega_u t + \chi \sin(\omega_u t)]. \quad (2.15)$$

Averaging,  $\int_0^{2\pi/\omega_u} dt(\dots)$ , eliminates the fast motion and gives

$$\frac{d\bar{\gamma}}{d\tau} = \frac{eEKL}{\bar{\gamma} mc^2} J_{n-1}(n\chi) \cos(n\bar{\xi} + \varphi - n\Delta v\tau), \quad (2.16)$$

where we have used  $\bar{\gamma}^2 \approx \bar{\gamma}^2$ .<sup>11</sup> For  $\vartheta = 0$ , and  $\chi = \Delta v = 0$ , (2.16) reduces to the well-known FEL result.<sup>11</sup> The electron phase with respect to the optical field is  $n\bar{\xi}$ . These phases evolve slowly and bunch to drive the optical wave coherently. The Bessel function describes the reduced coupling to the optical wave when  $\vartheta > 0$ . There is greater reduction in the higher harmonics. The factor  $n\Delta v$  modifies the resonance condition, or phase velocity, when the electromagnetic wave is viewed at a slight angle  $\vartheta$ . The form of (2.16) is a clear representation of the effects of misalignment ( $\vartheta > 0$ ). The complicated "fast" oscillations created by misalignment have been simply expressed as a new coupling constant  $J_{n-1}(n\chi)$ , and a new phase velocity  $n\Delta v$  experienced by the electrons.

Another useful form of (2.16) is the pendulum equation.<sup>33-35</sup> When  $N \gg 1$ , the electron energy  $\gamma$  is almost constant, and  $\bar{\xi} = \bar{v} = 4\pi N\dot{\gamma}/\gamma$ , where  $(\dot{\ })$  indicates the derivative with respect to  $\tau$ . So (2.16) may be written as

$$n\dot{\bar{v}} = n\ddot{\bar{\xi}} = |a_h| \cos(n\bar{\xi} + \varphi - n\Delta v\tau), \quad (2.17)$$

where the dimensionless optical-field strength is

$$|a_h| = \frac{4\pi NeKLE}{\gamma^2 mc^2} [nJ_{n-1}(n\chi)],$$

and  $\bar{v} = d\bar{\xi}/d\tau$  is the electron phase velocity. The pendulum equation (2.17) and even (2.16) can be written in the more usual form with the substitution  $v_s(\vartheta) = (\bar{v} - \Delta v)n$ ; then  $\xi_s(\vartheta) = (\bar{\xi} - \Delta v\tau)n$ . The pendulum equation can now be written in the standard form:

$$\dot{v}_s = \ddot{\xi}_s = |a_h| \cos(\xi_s + \varphi). \quad (2.18)$$

The physical meaning of (2.18) has been fundamental in the understanding of the FEL. We quickly review the

main features again to clarify the new definitions when  $\vartheta > 0$ . A beam of electrons occupies a range of initial conditions  $\zeta_0 = \zeta_s(0)$  and  $v_0 = v_s(0)$  in phase space at  $\tau = 0$ . If the beam is monoenergetic and all electrons propagate at the same angle  $\vartheta$ , then only one phase velocity  $v_0$  is populated. For short wavelengths, a uniform distribution of phases  $\zeta_0$  will cover every  $2\pi$  section of phase space. Bunching and coherent emission occur when the phase  $\zeta_s \approx \pi$  is overpopulated and the average electron energy  $\langle v_s \rangle$  decreases. In order to maintain an overpopulated phase for a significant time we must have  $|v_s| < \pi$ . Since the field strength  $|a_h|$  changes the rate at which each  $v_s$  evolves, we see that  $|a_h| < \pi$  implies weak fields and slight bunching, whereas  $|a_h| > \pi$  implies strong fields and strong bunching. If  $|a_h| \gg \pi$ , bunching is no longer possible over long times. Such strong fields reduce the amount of bunching, or gain, and lead to saturation.

The parameter  $v_s$  defines a resonant wavelength where there is optimum coupling between the electrons and light. This requires  $\lambda/n \approx \lambda_u(1 + K^2 + \gamma^2\vartheta^2)/2n\gamma^2$  which agrees with the expression for the wavelength emitted at angle  $\vartheta$  in (2.6) and establishes the equivalence between a skewed electron beam and resonator mode.

### C. The wave equation with imperfect helical trajectories

We now go on and develop the modified coupling of electrons to the self-consistent wave equation. The calculation follows and generalizes previous work.<sup>11,36</sup> The wave equation in the Coulomb gauge is

$$\left[ \nabla^2 - \frac{1}{c^2} \frac{\partial^2}{\partial t^2} \right] \vec{A}_n = -\frac{4\pi}{c} \vec{J}_T = 4\pi e \sum_j \vec{\beta}_T \delta^{(3)}(\vec{x} - \vec{r}_j), \quad (2.19)$$

where  $\vec{J}_T$  is the transverse electron current, and  $\vec{r}_j$  is the trajectory of the  $j$ th electron in the beam. When the form  $\vec{A}_n$  is substituted into (2.19), the slowly varying amplitude  $E(z, t)$  and phase  $\varphi(z, t)$  guarantees that higher order derivatives are small compared to single derivatives. The contribution of each electron is then proportional to  $[(K/\gamma)e^{i(k_u z + \psi)} - \vartheta e^{i\psi}]$ . This is the same phase behavior we saw in (2.13) during the derivation of the pendulum equation; the term proportional to  $\vartheta$  again oscillates fast, and can be averaged away. The argument  $(k_u z + \psi)$  is evaluated in the same way as in (2.14) to obtain the reduced coupling expressed by the Bessel function in (2.16). The complete sum in the current can be replaced by an average  $\langle \dots \rangle$  over sampled electrons if the electron density  $\rho$  is used as a weight factor.<sup>36</sup> The wave equation is then simplified to its final form by the substitution  $s = z - ct$  and  $\tau = ct/L$ .

$$\dot{a}_h = -j_h \langle e^{-i\zeta_s} \rangle, \quad (2.20)$$

where the dimensionless current density is

$$j_h = \frac{8\pi^2 N e^2 K^2 L^2 \rho}{\gamma^3 m c^2} [n J_{n-1}^2(n\chi)].$$

Together with (2.16) or (2.18), the self-consistent wave and electron equations of motion yield a powerful formulation

of the FEL problem. These equations are valid for weak or strong optical fields  $|a_h|$  with high or low gain. High gain effects occur when  $j_h \gg 1$ , and the fields must be integrated self-consistently. When  $j_h < 1$ , the gain is considered low and the field does not have to be integrated self-consistently. The equations can be easily extended to include short pulse effects,<sup>37</sup> multimode behavior,<sup>38,39</sup> and Coulomb forces.<sup>11</sup> In each case the modified coupling due to misalignment is expressed through the simple new coupling factor  $n J_{n-1}(n\chi)$ . Since the form of (2.18) and (2.20) remains the same as in the  $\vartheta = 0$  case, all the previously derived mathematical results remain unchanged in form.

The important expression of FEL low-gain ( $j_h \leq 1$ ) in weak fields ( $|a_h| \leq \pi$ ) can be straightforwardly calculated. Solving (2.18) and (2.20) together gives the gain, defined as  $(|a_h(1)|^2 - |a_h(0)|^2)/|a_h(0)|^2$ , in the  $n$ th harmonic at angle  $\vartheta$  with the initial electron beam at resonance parameter  $v_0$ .

$$G_h = j_h \frac{[2 - 2\cos(v_s) - v_s \sin(v_s)]}{v_s^3} = -\frac{j_h}{2} \frac{d}{dv_s} \left[ \frac{\sin^2(v_s/2)}{(v_s/2)^2} \right], \quad (2.21)$$

where we recall that  $v_s = v_0 - \Delta v(\vartheta)$ . The maximum gain occurs at  $v_s = 2.6$  and  $v_s = 0$  gives no gain. The gain bandwidth is  $|v_s| < 2\pi$  and the gain curve has the usual antisymmetric shape. Note that the gain spectrum is proportional to the slope of the spontaneous emission line-shape  $\sin^2(v_s)/v_s^2$ .

Figure 6 shows an intensity plot of  $G_h$  in the helical undulator versus the angle  $\gamma\vartheta$  and the dimensionless frequency  $\omega/2\gamma^2\omega_u$  for  $K=0.5$ . The brightest points (white) indicate peak gain of  $[8N(\pi eKL)^2 \rho / \gamma^3 m c^2] \times (0.135)$ , while the darkest points (black) indicate peak absorption, or a loss of  $[8N(\pi eKL)^2 \rho / \gamma^3 m c^2] \times (-0.135)$ . Zero gain is indicated by the intermediate grey shown in the scale at the top. The gain clearly follows the resonance condition  $v_s(\omega, \vartheta) \approx 0$  as did the spontaneous emission spectrum. At each harmonic, the shape of the gain curve in  $\omega$  is approximately determined by the slope of  $\sin^2[v_s(\omega)/2]/v_s^2(\omega)$  when  $N \gg 1$ , since the frequency dependence in  $j_h$  is relatively broad. Note that  $N = 10$  in Figs. 6 and 7 so that their features can be seen more easily; usually  $N \approx 100$ . In the fundamental, the gain far off axis remains comparable to the gain on axis. With  $K = 0.5$ , the off-axis gain in higher harmonics is small compared to the fundamental. Figure 7 is identical to Fig. 6, but with  $K = 1.0$ . The coupling, or gain, in higher harmonics is increased with respect to the fundamental.

### III. SPONTANEOUS EMISSION FROM PERFECT LINEAR TRAJECTORIES

The electron trajectories for the linearly polarized undulator (referred to as the "linear" case) are more complicated than in the helical case. Even with perfect injection there is fast oscillatory  $z$  motion which causes spontaneous emission on axis into the odd higher harmonics.<sup>10-15</sup> The magnetic field of a linear undulator near the axis is

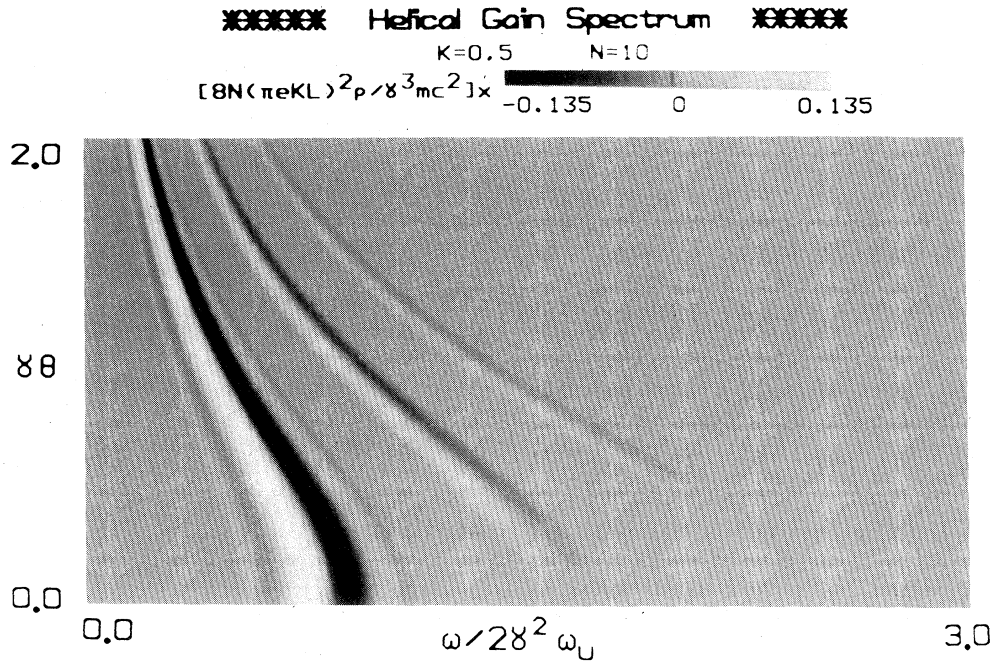


FIG. 6. FEL gain spectrum in a helical undulator is plotted for  $K = 0.5$  and  $N = 10$ . Black indicates peak absorption, or negative gain, while white indicates peak gain; the intermediate scale is indicated in grey  $\times [8N(\pi eKL)^2\rho/\gamma^3mc^2]$ . There is substantial gain off axis and the frequency  $\omega$  can be tuned over a large range with almost no decrease in coupling. At this low value of  $K$ , the gain in higher harmonics is much less than in the fundamental. There is no gain on axis except at the fundamental.

$$\vec{B}_I = (0, B \sin(k_u z), 0) \text{ for } 0 < z < L. \tag{3.1}$$

$$\vec{\beta}_T = \left[ -\frac{\sqrt{2}K}{\gamma} \cos(k_u z), 0, 0 \right], \tag{3.2}$$

For perfect injection, the Lorentz force equations (2.1) can be solved exactly to give

where  $K = e\bar{B}\lambda_u/2\pi mc^2$ , and now  $\bar{B} = B/\sqrt{2}$ . The elec-

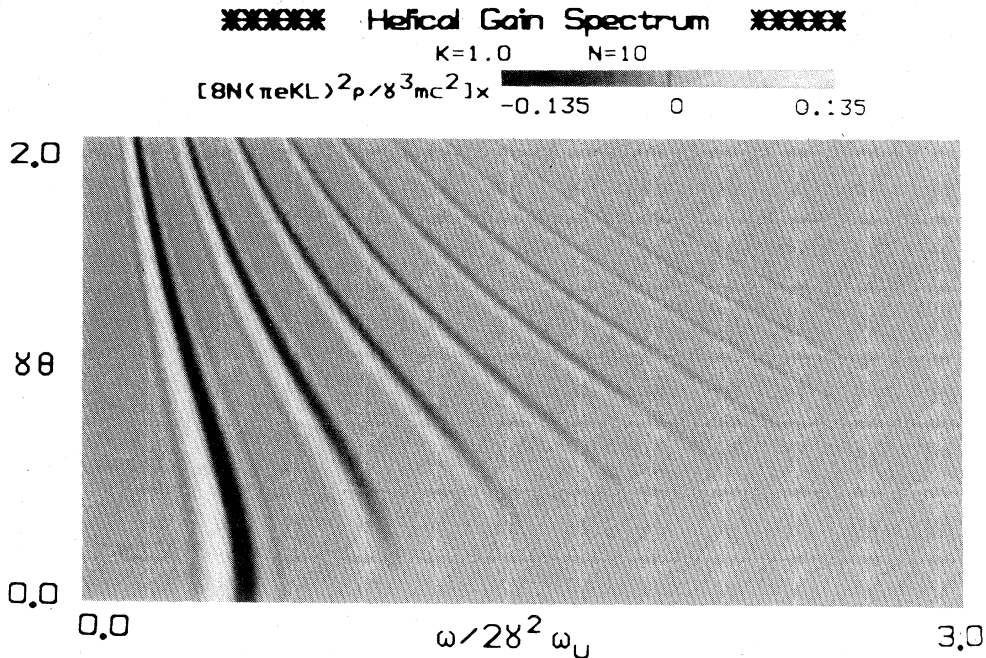


FIG. 7. FEL gain spectrum in a helical undulator is plotted for  $K = 1.0$  and  $N = 10$ . Again there is substantial gain off axis, but with this increased value of  $K$ , the gain in higher harmonics is now comparable to the gain in the fundamental. Comparison with Fig. 3 shows gain only occurs where there is spontaneous emission, since each process must roughly satisfy the resonance condition  $\nu_n \approx 0$ . As the optical resonator is tilted in angle  $\vartheta$ , the FEL can be tuned to a large range of frequencies with good coupling.



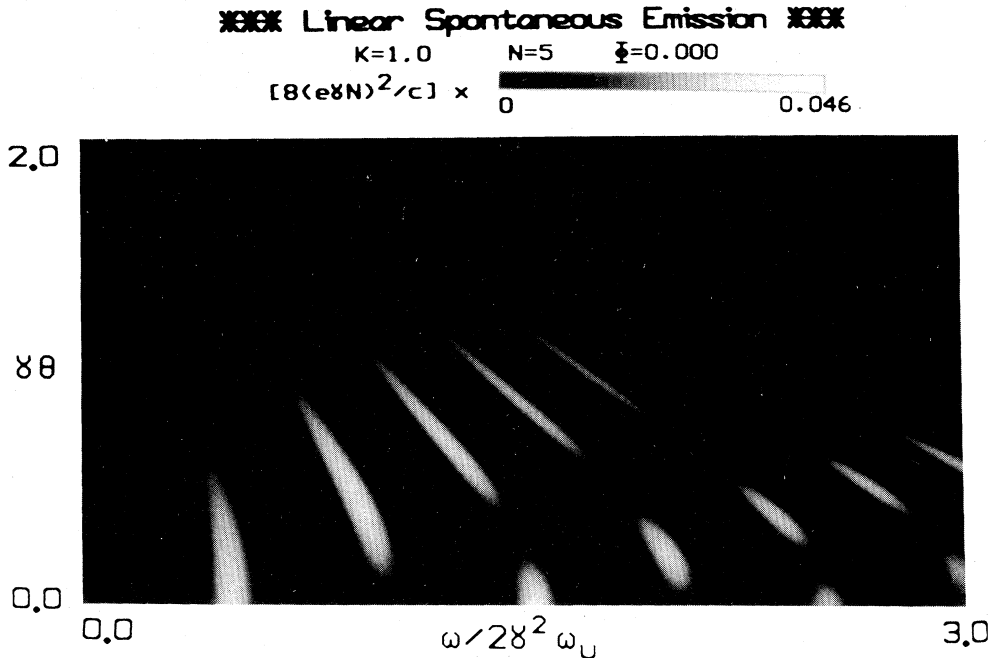


FIG. 9. FEL spontaneous emission intensity from a linear undulator is plotted for  $K=1.0$ ,  $N=5$ , and observed at  $\Phi=0$ . At this higher value of  $K$ , there is increased emission in several higher harmonics. Unlike the helical undulator case, the linear case has emission on axis in the odd harmonics  $n=1,3,5,\dots$ . In all harmonics, there is structure in the angle  $\vartheta$ , which gives a more complicated spectrum. This is because the motion in a linear undulator is more complicated than in the helical case.

case is the presence of odd harmonics at  $\vartheta=0$ , and the number of peaks in each harmonic as  $\gamma\vartheta$  is increased. The number of peaks in each harmonic over the full angular range is equal to the harmonic number  $n$ . These new features are due to the fast oscillatory term in the trajectory

even for perfect injection.

Figure 10 shows the intensity plot for  $K=1$ , but with the observation point rotated to  $\Phi=\pi/2$ . The emission in the even harmonics decreases sharply, and the structure in the odd harmonics disappears. The intensity plot for

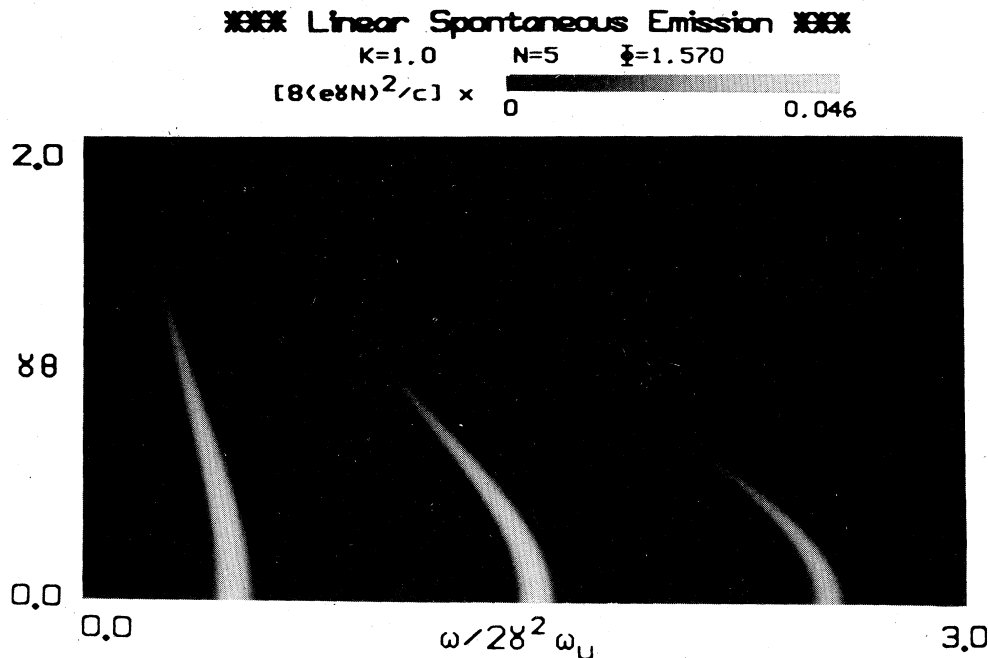


FIG. 10. FEL spontaneous emission intensity from a linear undulator is plotted for  $K=1.0$ ,  $N=5$ , and observed at  $\Phi=\pi/2$ . When the detector is moved to this observation point, the emission in the even harmonics  $n=2,4,6,\dots$  vanishes and the structure in the angle  $\vartheta$  is removed from the odd harmonics.

$\Phi = \pi$  is the same as for  $\Phi = 0$ ; see (3.5). In Figs. 8–10, the number of undulator periods ( $N = 5$ ) is smaller than typical to make the emission pattern more visible.

### A. Imperfect linear trajectories

The trajectories calculated here will include an imperfect injection angle which will give more complex fast oscillations. Solving (2.1) in the field (3.1) with more general constants of integration gives

$$\vec{\beta}_T = \left[ -\frac{\sqrt{2}K}{\gamma} \cos(k_u z) + \vartheta_x, \vartheta_y, 0 \right], \quad (3.6)$$

where  $\vartheta_x = \beta_x(0)/\beta_z(0) \approx \vartheta \cos(\Phi)$  and  $\vartheta_y = \beta_y(0)/\beta_z(0) \approx \vartheta \sin(\Phi)$  are constants of integration describing the injection angle. Unlike the helical case, the motion is not azimuthally symmetric so that the angles  $\vartheta_x$  and  $\vartheta_y$  have different effects on the mode coupling. The  $z$  motion is

$$\beta_z^2 = 1 - \gamma^{-2} - \frac{2K^2}{\gamma^2} \cos^2(k_u z) + \frac{2\sqrt{2}K\vartheta \cos(\Phi)}{\gamma} \cos(k_u z) - \vartheta^2, \quad (3.7)$$

where  $\vartheta^2 \approx \vartheta_x^2 + \vartheta_y^2$ . Average over an integral number of undulator wavelengths to separate the fast and slow oscillating terms as before. In the limit of  $\gamma \gg 1$  expand to order  $(K/\gamma)^2$  to get

$$\Delta\beta_z(t) \approx -\frac{K^2}{2\gamma^2} \cos(2\omega_u t) + \frac{\sqrt{2}K\vartheta \cos(\Phi)}{\gamma} \cos(\omega_u t), \quad (3.8)$$

$$\Delta z(t) \approx -\frac{K^2\lambda_u}{8\pi\gamma^2} \sin(2\omega_u t) + \frac{K\lambda_u\vartheta \cos(\Phi)}{\sqrt{2}\pi\gamma} \sin(\omega_u t),$$

where  $\bar{\beta}_z = 1 - (1 + K^2)/2\gamma^2 - \vartheta^2/2 \approx 1$ . Now there are two kinds of fast oscillations and their amplitudes can be comparable in typical cases. The effect of  $\vartheta_y > 0$  alone is a change in  $\bar{\beta}_z$  and the resonance condition, but there are no additional oscillations.

As for the helical case, the fast  $z$  motion becomes important when it is comparable to optical wavelength  $\lambda$ . This occurs when

$$k\Delta z \approx -\frac{K^2\lambda_u}{4\lambda\gamma^2} \sin(2\omega_u t) + \frac{\sqrt{2}K\lambda_u\vartheta \cos(\Phi)}{\lambda\gamma} \sin(\omega_u t) \approx -\xi \sin(2\omega_u t) + \sqrt{2}\chi \cos(\Phi) \sin(\omega_u t) \approx 1, \quad (3.9)$$

where  $\xi = K^2/2(1 + K^2 + \gamma^2\vartheta^2)$  and  $\chi = 2K\gamma\vartheta/(1 + K^2 + \gamma^2\vartheta^2)$ . For  $K \approx 1$  and  $\gamma\vartheta_x \approx \gamma\vartheta \cos(\Phi) \approx 1$  the fast  $z$  motion can be important.

### B. The pendulum and wave equation with imperfect linear trajectories

To calculate the coupling for the linear case we must introduce the electromagnetic wave. The vector potential of the linearly polarized optical field is

$$\vec{A}_n = \frac{E}{nk_1} [\sin(\psi), 0, 0], \quad (3.10)$$

where again  $\psi = nk_1 z - n\omega_1 t + \varphi$ . Substitution into the energy equation gives

$$\frac{d\gamma}{dt} = \frac{eEK}{\sqrt{2}\gamma mc} [\cos(k_u z + \psi) + \cos(k_u z - \psi)] - \frac{eE\vartheta_x}{mc} \cos(\psi). \quad (3.11)$$

The three terms on the right in (3.11) oscillate at different frequencies. The phases  $(k_u z - \psi)$  and  $\psi$  oscillate  $\approx \gamma^2$  times faster than  $(k_u z + \psi)$  and can be averaged away as in (II B). The important slow, resonant phase  $(k_u z + \psi)$  may be rewritten as

$$\psi + k_u z = n\bar{\xi} + \varphi - (n-1)\omega_u t - n\xi \sin(2\omega_u t) + n\sqrt{2}\chi \cos(\Phi) \sin(\omega_u t) - n\Delta\nu\tau, \quad (3.12)$$

where  $\bar{\xi}$  and  $\Delta\nu$  are defined below (2.14). Inserting (3.12) into (3.11) and averaging over a number of discrete undulator periods to eliminate the fast motion we get

$$\frac{d\bar{\gamma}}{d\tau} = \frac{eKEL}{\bar{\gamma}mc^2} \left[ \frac{1}{\sqrt{2}} \sum_{n'=-\infty}^{\infty} J_{n'}(n\xi) [J_{2n'+n+1}(nZ) + J_{2n'+n-1}(nZ)] \right] \cos(n\bar{\xi} + \varphi - n\Delta\nu\tau), \quad (3.13)$$

where  $Z = \sqrt{2}\chi \cos(\Phi)$ . When  $\vartheta = 0$ , then  $\chi = \Delta\nu = 0$  and (3.13) reduces to the previous result describing gain at odd higher harmonics.<sup>11,13</sup> When  $N \gg 1$ , we can introduce the variables  $v_s(\vartheta) = n(\bar{v} - \Delta\nu)$  and  $\xi_s(\vartheta) = n(\bar{\xi} - \Delta\nu\tau)$  so that we get the pendulum equation

$$\dot{v}_s = \ddot{\xi}_s = |a_I| \cos(\xi_s + \varphi), \quad (3.14)$$

where the dimensionless field strength is now

$$|a_I| = \frac{4\pi NeKEL}{\gamma^2 mc^2} \left[ \frac{n}{\sqrt{2}} \sum_{n'=-\infty}^{\infty} J_{n'}(n\xi) [J_{2n'+n+1}(nZ) + J_{2n'+n-1}(nZ)] \right].$$

The wave equation can now be derived with the same procedure as in the helical case. In its simplified form we have

$$\dot{a}_I = -j_I \langle e^{-i\xi_s} \rangle, \quad (3.15)$$

where the dimensionless current density is now

$$j_l = \frac{8\pi^2 N e^2 K^2 L^2 \rho}{\gamma^3 m c^2} \left[ n \left[ \sum_{n'=-\infty}^{\infty} J_{n'}(n\xi) [J_{2n'+n+1}(nZ) + J_{2n'+n-1}(nZ)] \right]^2 \right],$$

where  $Z = \sqrt{2}\chi \cos(\Phi)$ . The form of the wave and pendulum equations are exactly the same as in the helical undulator case so that the all results for each may be directly related with the substitution  $j_h \rightarrow j_l$  and  $a_h \rightarrow a_l$ . The new coupling is expressed in the Bessel functions of these variables. The gain  $G_l$  is determined by replacing  $j_h \rightarrow j_l$  in (2.21):

$$G_l = j_l \frac{[2 - 2 \cos(v_n) - v_n \sin(v_n)]}{v_n^3} \tag{3.16}$$

Figure 11 shows the gain  $G_l$  in the linear undulator as a function of angle  $\gamma\vartheta$  and the dimensionless frequency  $\omega/2\gamma^2\omega_u$  for  $K=0.5$  and  $\Phi=0$ . The brightest points (white) indicate peak gain of  $[8N(\pi eKL)^2\rho/\gamma^3mc^2] \times (0.12)$ , while the black points indicate negative this value; intermediate values are shown in the grey scale at the top. Recall that  $K$  in the linear case is  $\sqrt{2}$  times smaller than in the helical case for the same peak field  $B$ ; this means that for the same weak undulator field  $B$ , such that  $K \ll 1$ , the gain in the linear undulator case is only half of the gain in the helical undulator case. The detailed shape of the gain curve is the same as in the linear case, but the large scale structure in  $(\vartheta, \omega)$  differs because of new coupling factor  $j_l$ . Now the odd harmonics have gain on axis at  $\vartheta=0$ , and in each harmonic there is more structure with changing angle  $\gamma\vartheta$ .

Figure 12 shows the gain for  $K=1.0$  and  $\Phi=0$ . The peak gain (white) indicates  $[8N(\pi eKL)^2\rho/\gamma^3mc^2] \times (0.10)$ . The figure shows that the amount of gain in higher harmonics is increased just as in the helical case. The structure of the gain in each harmonic is more clear because it's brighter compared to the fundamental.

Figure 13 shows the gain for  $K=1.0$ , but the observation angle is rotated to  $\Phi=\pi/2$ . The peak gain (white) indicates  $[8N(\pi eKL)^2\rho/\gamma^3mc^2] \times (0.124)$ . The gain in even harmonics is now greatly reduced for all values of  $\gamma\vartheta$ . The gain for  $\Phi=\pi$  is the same as for  $\Phi=0$ . This azimuthal structure in the gain angular spectrum can cause excitation of higher order modes in a spherical mirror resonator.<sup>38,39</sup>

IV. ENERGY AND ANGULAR DISTRIBUTIONS

The new couplings calculated here may be used to extend the tunable range of an FEL, but may also be used to analyze the effects of emittance or misalignment of an electron beam. Excess emittance is like a large energy spread which destroys the resonance condition and decreases gain. Electrons cannot be effectively bunched within an optical wavelength for an extended interaction time if there is significant spread in their  $z$  velocities. The gain reduction in higher harmonics is larger than in the fundamental simply because the wavelength is shorter;

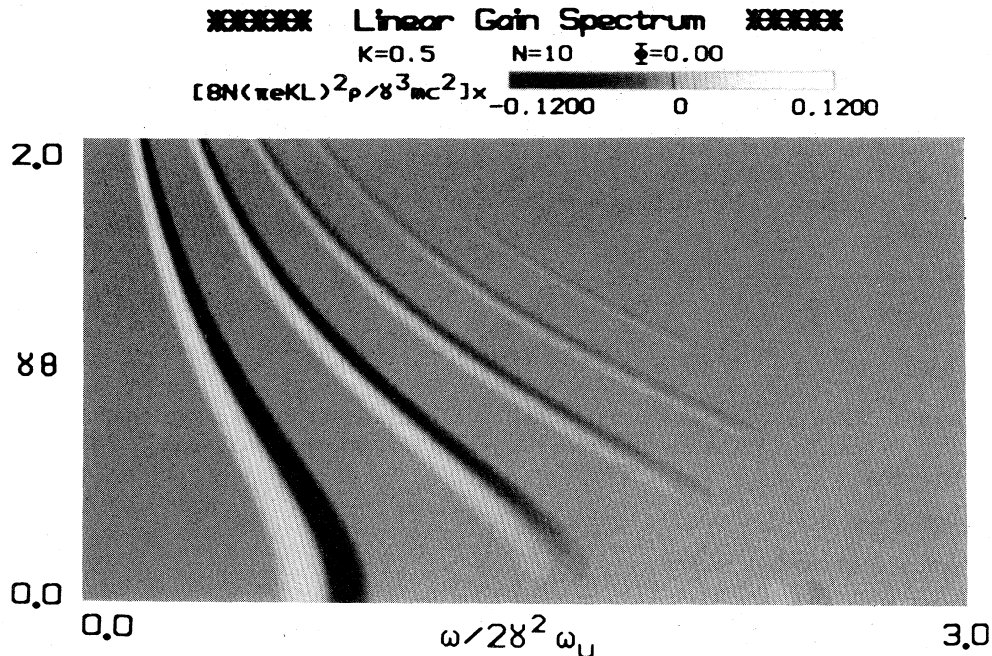


FIG. 11. FEL gain spectrum in a linear undulator is plotted for  $K=0.5$ ,  $N=10$ , and  $\Phi=0$ . Black indicates peak absorption, while white indicates peak gain; the intermediate scale is indicated in grey  $\times [8N(\pi eKL)^2\rho/\gamma^3mc^2]$ . Again, there is substantial gain off axis in several harmonics, but unlike the helical case, there is now gain on axis in the odd harmonics  $n = 1, 3, 5, \dots$

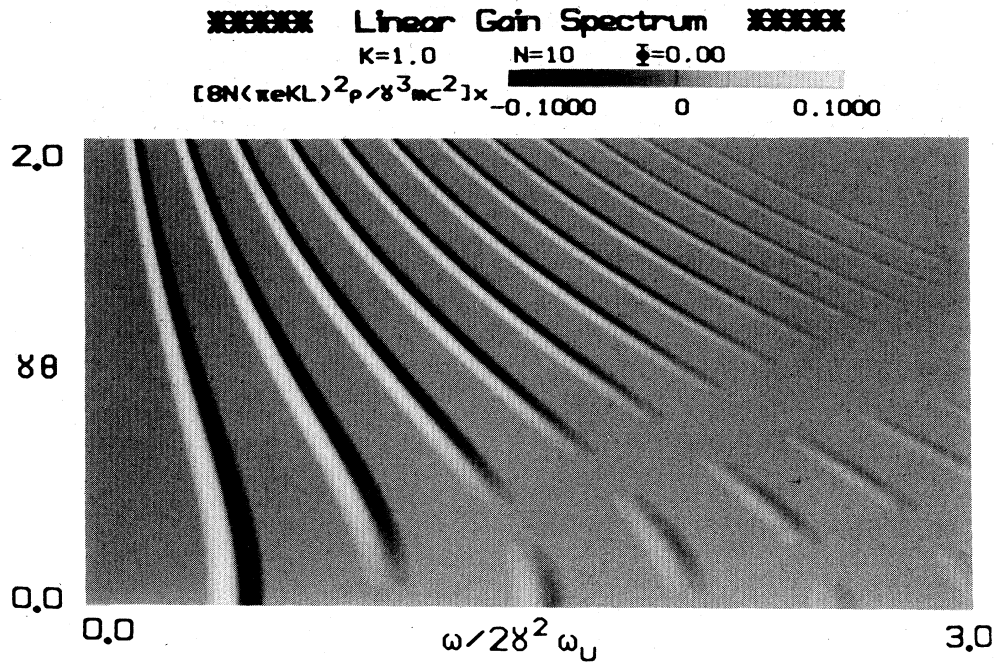


FIG. 12. FEL gain spectrum in a linear undulator is plotted for  $K=1.0$ ,  $N=10$ , and  $\Phi=0$ . At this higher value of  $K$ , there is much more gain available in the higher harmonics. The structure of the gain spectrum as a function of  $\vartheta$  can lead to some interesting effects when the optical wavefront is amplified.

this is the primary difficulty for FELs operating in higher harmonics.

From the definition of  $\nu_n$ , a variation in energy  $\delta\gamma$  causes a variation in the resonance of  $\delta\nu \approx 4\pi N\delta\gamma/\gamma n$ .<sup>13</sup> A beam with  $\delta\nu \approx \pi$  suffers a gain decrease of about half compared to the monoenergetic case. Emittance  $\epsilon$  and

thus the associated angular spread  $\sigma$ , affects the  $z$  velocity of electron and also alters the resonance condition. An electron traveling at an angle  $\vartheta$  has a change in resonance of  $\delta\nu = -2\pi N\gamma^2\vartheta^2/(1+K^2)n$ .<sup>13</sup> In terms of emittance this is  $\delta\nu = -N\gamma^2\epsilon^2/r^2(1+K^2)n$ , where  $r$  is the electron beam radius.

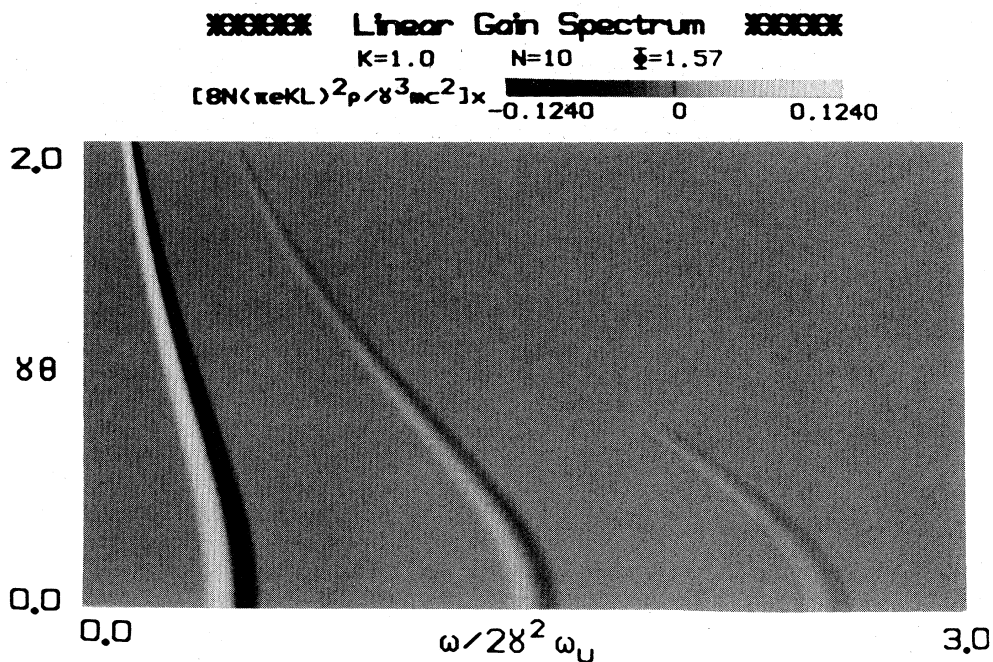


FIG. 13. FEL gain spectrum in a linear undulator is plotted for  $K=1.0$ ,  $N=10$ , and  $\Phi=\pi/2$ . At this observation angle, the gain in the even harmonics  $n=2,4,6,\dots$  and the angular structure of the odd harmonics disappears.

An electron beam with poor quality has a range of initial resonance conditions  $\nu_0$ . In our formulation, an electron's initial coordinates are specified by  $\xi_0 = \xi(0)$ ,  $\nu_0 = \nu(0)$ , and  $\vartheta$ . We neglect  $\vartheta_y$  here for simplicity. The average over sampled electrons in the wave equation must be interpreted as  $\langle \cdots \rangle = \langle \langle \langle \cdots \rangle_{\xi_0} \rangle_{\nu_0} \rangle_{\vartheta}$ . Typically, these separate averages over  $\xi_0$ ,  $\nu_0$ , and  $\vartheta$  are not correlated and the average  $\langle \cdots \rangle_{\xi_0}$  is taken to be uniform,  $\int_0^{2\pi} (\cdots) d\xi_0 / 2\pi$ . The average  $\langle \cdots \rangle_{\nu_0}$  may describe a Gaussian energy spread, for example. The angular spread due to emittance can be taken to be Gaussian

$$\langle \cdots \rangle_{\vartheta} = (2/\pi)^{1/2} \int_0^{\infty} d(\vartheta/\sigma) e^{-\vartheta^2/2\sigma^2} (\cdots),$$

where  $\sigma \ll \pi$  is the characteristic rms angle. The electron beam here is centered on axis and the spread in angles is due to emittance.

When the spread  $\sigma$  is small enough so that  $\Delta\nu \ll \pi$  for all electrons, there is no significant spread of resonance conditions in the electron beam and the average  $\langle \cdots \rangle_{\vartheta}$  can be done analytically. When  $\gamma\sigma \ll 1$ , both  $\Delta\nu \ll \pi$ , and  $\chi \ll 1$  can be satisfied, and we expand in the small argument  $\chi$ . On axis the gain from a perfect beam ( $\sigma=0$ ) only occurs at the fundamental ( $n=1$ ) in the helical case, and only at the odd harmonics ( $n=1,3,5,\dots$ ) in the linear case. These gains are reduced by the presence of emittance. In the helical case

$$G_h(\sigma) = G_h(0)(1 - X^2/2 + \cdots), \quad (4.1)$$

where  $X = 2K\gamma\sigma/(1+K^2)$ ,  $G_h(0)$  is the on-axis ( $\vartheta=0$ ) gain for the perfect beam in (2.21), and  $n=1$ . In the linear case

$$G_l(\sigma) = G_l(0)[1 - (nX)^2 + \cdots], \quad (4.2)$$

where  $G_l(0)$  is the on-axis gain ( $\vartheta=0$ ) for a perfect beam in (3.16), and  $n=1,3,5,\dots$

In addition to decreasing the gain at those  $(\omega, \vartheta)$  points where gain is nonvanishing, the existence of emittance creates new gain where there was no gain. This occurs because the electron beam's angular spread mixes off-axis couplings in  $j_l$  and  $j_h$ . In the helical case, the new gain occurs at  $n=2,3,4,\dots$  and is given by

$$G_h(\sigma) \approx G_h(0) \frac{(2n-3)!!}{[(n-1)!]^2} \left[ \frac{nK\gamma\sigma}{1+K^2} \right]^{2(n-1)}. \quad (4.3)$$

In the linear case, the new gain occurs at  $n=2,4,6,\dots$  and is given by

$$G_l(\sigma) \approx G_l(0) \left[ \frac{\sqrt{2}nK\gamma\sigma \cos(\Phi)}{1+K^2} \right]^2. \quad (4.4)$$

## V. CONCLUSIONS

In both the helical and linear undulator cases we saw that when  $K$  increases, a larger number of harmonics appear in the spectrum. The harmonics become more closely spaced and the spectrum starts to resemble the broadband spectrum of a bending magnet which is useful as a synchrotron radiation source.<sup>29,30</sup> A simple argument gives an understanding of the transition from the undula-

tor radiation spectrum to the bending magnet spectrum. As the undulator field strength  $B$  is increased, electrons deviate further from their linear path along the  $z$  axis. When  $B$  is large enough an electron would be trapped in an orbit smaller than the undulator wavelength  $\lambda_u$ ; trajectories along the undulator are no longer possible. In a bending magnet with constant field  $B$  the bending radius of a relativistic electron is  $\rho \approx 2\pi\gamma mc^2/eB$ .<sup>21</sup> The field at which  $\rho \sim \lambda_u$  means that  $K \sim \gamma$ . At this limit  $\beta_z \rightarrow 0$  in the helical trajectories of (2.4), and the  $K/\gamma$  expansion breaks down in the linear trajectories of (3.4). The limit  $K \sim \gamma$  indicates that the electron deflection angle is larger than the radiation cone, so that the cone passes rapidly through a detector at any position and produces a broadband spectrum. The synchrotron spectrum from an electron in a circular orbit of radius  $\rho$ <sup>21</sup> is

$$\frac{d^2I}{d\Omega d\omega} = \left[ \frac{3e^2\gamma^2}{\pi^2c} \right] \left[ \frac{\omega\rho}{3\gamma^3c} \right]^2 (1 + \gamma^2\vartheta^2)^2 \times \left[ K_{2/3}^2(\Psi) + \frac{\gamma^2\vartheta^2}{1 + \gamma^2\vartheta^2} K_{1/3}^2(\Psi) \right], \quad (5.1)$$

where  $\Psi = (\omega\rho/3\gamma^3c)(1 + \gamma^2\vartheta^2)^{3/2}$ , and  $K_{1/3}, K_{2/3}$  are modified Bessel functions. Figure 14 shows an intensity plot of (5.1) versus  $\gamma\vartheta$  and the dimensionless frequency  $\omega\rho/3\gamma^3c$ . The peak intensity (white) indicates an emission of  $[3e^2\gamma^2/\pi^2c] \times 0.37$ . The spectrum is featureless compared to the undulator spectrum and the emitted energy drops off at the characteristic angle  $\gamma\vartheta \approx 0.5$  and the characteristic frequency  $\omega\rho/3\gamma^3c \approx 1$ . Comparing the synchrotron emission rate in (5.1) to the undulator emission rates in (2.5) and (3.5), we note that the undulators radiate  $N^2$  times the energy into an element  $d\Omega d\omega$ . The total emission is more nearly equal since a synchrotron source covers more elements  $d\Omega d\omega$  as can be seen in the figures.

Another point deserving comment concerns the Madey theorem.<sup>22</sup> The Madey theorem states that the FEL gain spectrum is proportional to the slope of the spontaneous emission spectrum. A straightforward application of the theorem to the spectra presented here shows that this is not the case for  $\vartheta > 0$ . The gain off axis is not proportional to the slope of the spontaneous emission, and the original derivation of the Madey theorem only applies on axis. It may be possible, in principle, to generalize the theorem to off-axis propagation, but this effort must be weighed against making the direct calculation as is done here. Our experience is that the direct calculation appears more clear and less difficult.

An application of the gain calculations presented in this paper is to use the higher harmonics to extend the tunable range of an FEL to higher frequencies. The angular gain spectrum in each harmonic can, in turn, be used to tune the laser to lower frequencies. See Figs. 6, 7, and 11–13. In combination, these two tricks can significantly extend the tunable spectrum of an FEL without changing the electron energy. Since there is often a reduction of gain in off-axis higher harmonics, it is important to start with respectable gain in the fundamental on axis. The amount of reduction depends on  $K$  and the harmonic number  $n$ ; if

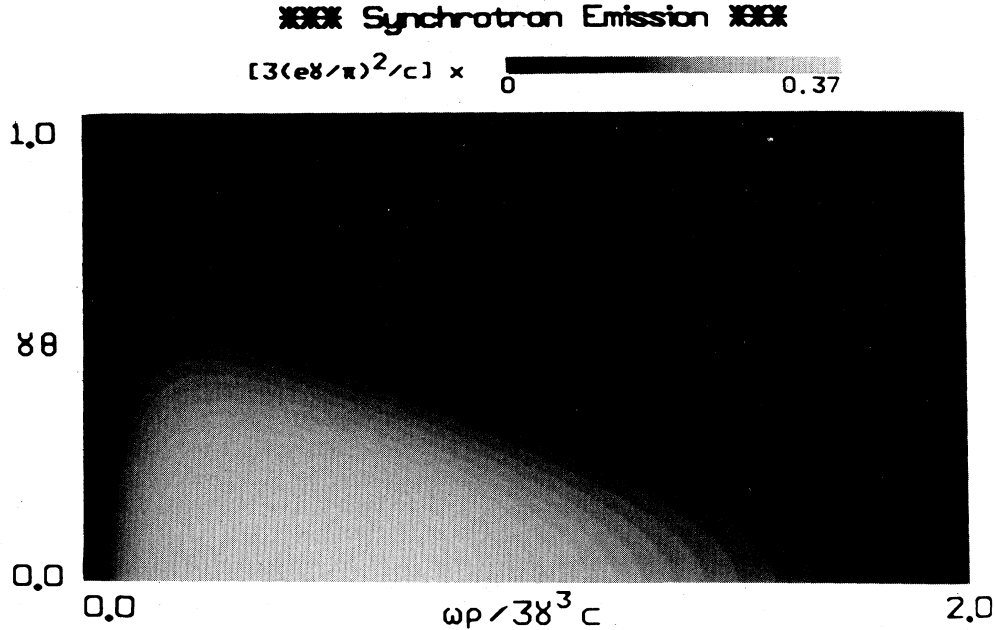


FIG. 14. Synchrotron spontaneous emission spectrum is plotted as a function of  $\gamma \vartheta$  and frequency  $\omega\rho/3\gamma^3 c$  for an electron in a path of radius  $\rho$ . The intensity scale is indicated in grey  $\times [3(e\gamma/\pi)^2/c]$ . In contrast to the undulator cases, the synchrotron spectrum is broad in both frequency and angle. The characteristic angle is  $\vartheta \approx 0.5/\gamma$ , and the characteristic frequency is  $3\gamma^3 c/\rho$ . While the total energy emitted is comparable to the undulators, the peak emission is less than an undulator by  $\times N^{-2}$ .

the undulator has  $K \approx 1$ , then the reduction in gain for the first few harmonics is not too large. The electron beam quality must improve in proportion to the harmonic number  $n^{-1}$  in order to maintain optimum coupling. Specific limitations are given in the last section.

The coupling factors calculated assumed a plane-wave form for the optical field. The plane-wave approximation is valid when the Rayleigh range  $z_0$  of the optical wavefront is much greater than the undulator length  $z_0 \gg L$ . The Rayleigh range is the distance over which the optical wavefront propagates as diffraction doubles its transverse area. Some aspects of the resonator mode problem can be incorporated in the electron and wave equations of motion in a simple way,<sup>38</sup> but as the angle  $\vartheta$  is increased in order to tune the FEL, we must be aware of the resonator mode's transverse dimension. See the schematic in Fig. 1. The waist area of the fundamental mode is  $\pi\omega_0^2 = z_0\lambda$  so that the characteristic angle of the mode is estimated by  $\vartheta_m \approx (\lambda/z_0)^{1/2}$ . It is often possible to use the undulator length  $L$  as an estimate of  $z_0$ . Then, a simple approximate form is  $\vartheta_m \approx 1/\gamma N^{1/2}$ . Note that  $\vartheta_m$  is typically smaller than the spontaneous emission cone  $\gamma^{-1}$ . Since angles like  $\vartheta \approx \gamma^{-1}$  are needed to change the optical wavelength significantly, staying within the resonator mode can place an important restriction on the tunable range.

It is also possible to make  $z_0 \gg L$  so that the mode area is wide enough to provide a large range of angles. But an FEL design, where the optical mode area is much larger than the electron beam cross section, suffers a serious reduction in gain because of this mismatch.<sup>18,32</sup> There are several practical aspects of the FEL design that have not been included in the discussion here. Our goal has been to evaluate the new coupling factors in a way that allows im-

mediate generalization to include the many other concepts already understood in FELs. These improvements are a natural extension of the work presented here.

Although no measurement of off-axis gain has been reported experimentally, higher harmonic emission on axis has been observed. Three of the four FEL experiments reported have observed emission at harmonics just above the fundamental.<sup>2-4</sup> Another experiment<sup>40</sup> has measured gain on-axis in the third harmonic of a linearly polarized undulator.

An example of an FEL system which could make good use of higher harmonics is a low-energy microtron. Such an FEL system has good electron quality, is small, compact, and relatively inexpensive. But because of the low-electron energy, say  $\gamma \approx 8$ , the FEL tends to work at rather long wavelengths and the use of higher harmonics can extend the operation to shorter wavelengths. Generally, the goals of high gain, large  $K$ , and good electron beam quality are common to all FEL work, so that the use of higher harmonics should become more wide spread in the future. The choice of an undulator with only a few periods is an advantage, since the characteristic mode angle  $1/\gamma N^{1/2}$  allows large excursions in  $\vartheta$ . The higher-harmonics gain mechanism can also be used to achieve coherent emission in several harmonics at the same time.

#### ACKNOWLEDGMENTS

We are grateful for helpful conversations with A. Renieri and J. Gallardo, and for the support from the U.S. Air Force Office of Scientific Research Grant No. AFOSR-84-0079 and the U.S. Office of Naval Research Grants Nos. N00014-81-K-0809 and N00014-81-C-2349.

- <sup>1</sup>S. Benson, D. A. G. Deacon, J. N. Eckstein, J. M. J. Madey, K. Robinson, T. I. Smith, and R. Taber, *Bendor Free Electron Laser Conference*, Proceedings of the Bendor Free Electron Laser Conference, Bendor, France, 1982 [J. Phys. (Paris) Colloq. **44**, C1-353 (1983)].
- <sup>2</sup>M. Billardon, P. Elleaume, J. M. Ortega, C. Bazin, M. Bergher, M. Velghe, Y. Petroff, D. A. G. Deacon, K. E. Robinson, and J. M. J. Madey, Phys. Rev. Lett. **51**, 1652 (1983).
- <sup>3</sup>J. A. Edighoffer, G. R. Neil, C. E. Hess, T. I. Smith, S. W. Fornaca, and H. A. Schwettman, Phys. Rev. Lett. **52**, 344 (1984).
- <sup>4</sup>R. W. Warren, B. E. Newman, W. E. Stein, J. G. Winston, R. L. Sheffield, M. T. Lynch, J. C. Goldstein, M. C. Whitehead, O. R. Norris, G. Luedemann, T. O. Gibson, and G. M. Humphrey, in Proceedings of the Sixth International Conference on Lasers and Applications, San Francisco, 1983 (STS Press, McLean, Virginia, 1984).
- <sup>5</sup>*Bendor Free Electron Laser Conference*, Proceedings of the Bendor Free Electron Laser Conference, Bendor, France, 1982 [J. Phys. (Paris) Colloq. **44**, C1-353 (1983)].
- <sup>6</sup>Special issues, IEEE J. Quantum Electron. **QE-17**, August (1981); **QE-19**, March (1983).
- <sup>7</sup>*Physics of Quantum Electronics*, edited by S. F. Jacobs *et al.* (Addison-Wesley, Reading, Mass., 1978–1982), Vols. 5, 7–9.
- <sup>8</sup>*Free Electron Lasers*, Vol. 18 of *Ettore Majorana International Science Series, Physical Sciences*, edited by S. Martellucci and A. N. Chester (Plenum, New York, 1983).
- <sup>9</sup>*Free-Electron Generators of Coherent Radiation*, Proceedings of Free-Electron Generators of Coherent Radiation, Orcas Island Washington, 1983, edited by C. A. Brau, S. F. Jacobs, and M. O. Scully (The Society for Photo-Optical Instrumentation Engineers, Washington, D.C., 1984), Vol. 453.
- <sup>10</sup>J. M. J. Madey and R. C. Taber, in *Physics of Quantum Electronics*, edited by S. F. Jacobs *et al.* (Addison-Wesley, Reading, Mass., 1980), Chap. 30.
- <sup>11</sup>W. B. Colson, IEEE J. Quantum Electron. **QE-17**, 1417 (1981).
- <sup>12</sup>R. Coisson, IEEE J. Quantum Electron. **QE-17**, 1409 (1981).
- <sup>13</sup>W. B. Colson, Phys. Rev. A **24**, 639 (1981).
- <sup>14</sup>F. Ciocci, G. Dattoli, and A. Renieri, Nuovo Cimento Lett. **34**, 341 (1982).
- <sup>15</sup>N. Al-Abawi, G. T. Moore, and M. O. Scully, Phys. Rev. A **24**, 3143 (1981).
- <sup>16</sup>M. V. Fedorov, Usp. Fiz. Nauk. **134**, 213 (1981) [Sov. Phys.—Usp. **24**, 801 (1981)]; D. F. Zaretskii, E. A. Neresov, and M. V. Fedorov, Zh. Eksp. Teor. Fiz. **80**, 999 (1981) [Sov. Phys.—JETP **53**, 508 (1981)].
- <sup>17</sup>M. V. Fedorov and S. Stenholm, Opt. Commun. **49**, 355 (1984).
- <sup>18</sup>J. M. J. Madey, J. Appl. Phys. **42**, 1906 (1971).
- <sup>19</sup>W. H. Louisell, J. Lam, D. A. Copeland, and W. B. Colson, Phys. Rev. A **19**, 288 (1979).
- <sup>20</sup>W. B. Colson, Ph.D. thesis, Stanford University, 1977.
- <sup>21</sup>J. D. Jackson, *Classical Electrodynamics* (Wiley, New York, 1975).
- <sup>22</sup>J. M. J. Madey, Nuovo Cimento B **50**, 64 (1979).
- <sup>23</sup>J. Schwinger, Phys. Rev. **75**, 1912 (1949).
- <sup>24</sup>G. A. Schott, *Electromagnetic Radiation* (Cambridge University, London, 1912).
- <sup>25</sup>J. P. Blewett and R. Chasman, J. Appl. Phys. **48**, 2692 (1977).
- <sup>26</sup>P. Diament, Phys. Rev. A **23**, 2537 (1981).
- <sup>27</sup>D. F. Alferov, Yu. A. Bashmakov, and E. G. Bessonov, Proc. P. N. Lebedev Phys. Inst. (Acad. Sci. USSR) **80**, 97 (1976).
- <sup>28</sup>B. M. Kincaid, J. Appl. Phys. **48**, 2684 (1977).
- <sup>29</sup>Phys. Today **34** (5), Special Issue (1981).
- <sup>30</sup>M. L. Perlman, E. M. Rowe, and R. E. Watson, Phys. Today **27** (7), 30 (1974).
- <sup>31</sup>S. K. Ride and W. B. Colson, Stanford University High Energy Physics Lab Report No. 858 (unpublished).
- <sup>32</sup>G. Dattoli and A. Renieri, in *Experimental and Theoretical Aspects of the Free Electron Laser*, in Vol. 4 of *Laser Handbook*, edited by M. L. Stitch and M. S. Bass (North-Holland, Amsterdam, in press).
- <sup>33</sup>W. B. Colson, Phys. Lett. **64A**, 190 (1977).
- <sup>34</sup>A. Bambini and A. Renieri, Nuovo Cimento Lett. **21**, 399 (1978).
- <sup>35</sup>V. N. Baier and A. I. Milstein, Phys. Lett. **65A**, 319 (1978).
- <sup>36</sup>W. B. Colson and S. K. Ride, Phys. Lett. **76A**, 379 (1980).
- <sup>37</sup>W. B. Colson and A. Renieri, J. Phys. (Paris) Colloq. **44**, C1-11 (1983).
- <sup>38</sup>W. B. Colson and P. Elleaume, Appl. Phys. B **29**, 101 (1982).
- <sup>39</sup>W. B. Colson and J. L. Richardson, Phys. Rev. Lett. **50**, 1050 (1983).
- <sup>40</sup>M. Biagini, R. Boni, S. De Simone, S. Guiducci, M. Preger, M. Serio, S. Tazzari, F. Tazzioli, S. Trillo, M. Vescovi, M. Ambrosio, G. C. Barbarino, M. Castellano, N. Cavallo, F. Cevenini, M. R. Masullo, P. Patteri, R. Rinzivillo, and S. Solimeno, *Free-Electron Generators of Coherent Radiation*, Proceedings of Free-Electron Generators of Coherent Radiation, Orcas Island Washington, 1983 edited by C. A. Brau, S. F. Jacobs, and M. O. Scully (The Society for Photo-Optical Instrumentation Engineers, Washington, D.C., 1984), Vol. 453, p. 275.

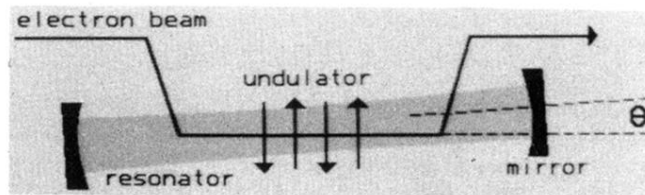


FIG. 1. FEL schematic shows an electron beam propagating through a periodic undulator, but with the optical resonator tilted at an angle  $\vartheta$ .

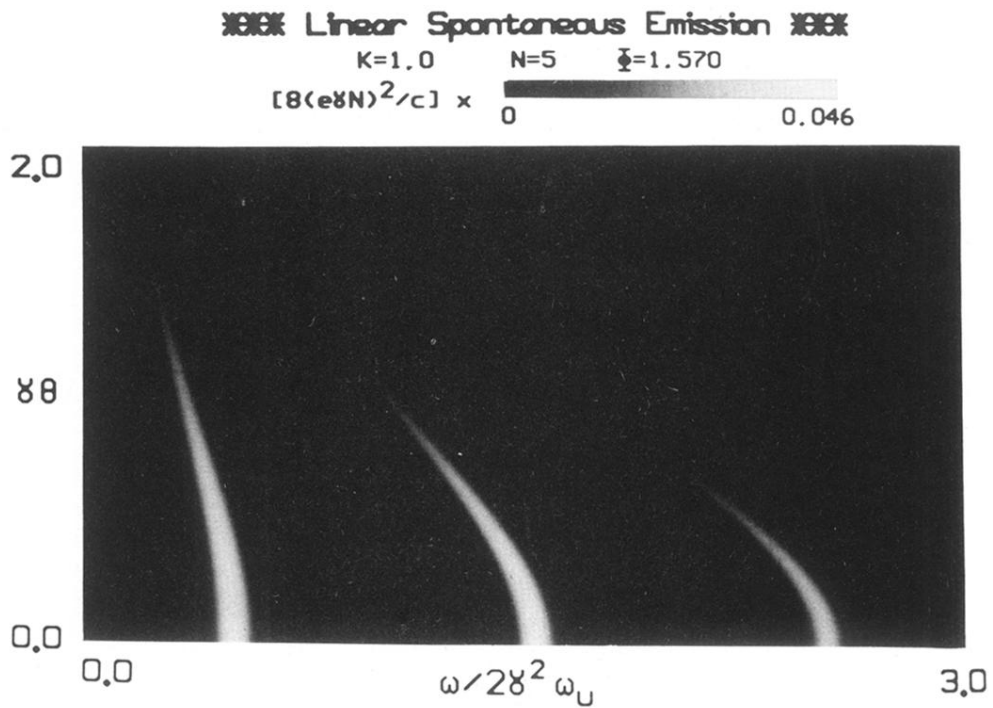


FIG. 10. FEL spontaneous emission intensity from a linear undulator is plotted for  $K=1.0$ ,  $N=5$ , and observed at  $\Phi=\pi/2$ . When the detector is moved to this observation point, the emission in the even harmonics  $n=2,4,6,\dots$  vanishes and the structure in the angle  $\vartheta$  is removed from the odd harmonics.

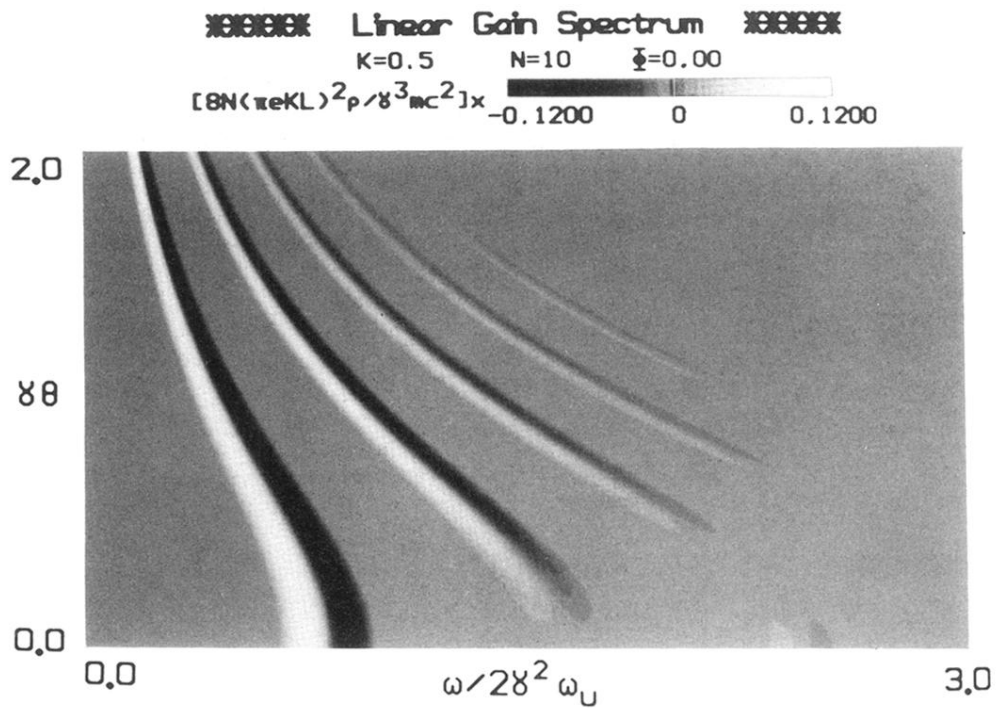


FIG. 11. FEL gain spectrum in a linear undulator is plotted for  $K=0.5$ ,  $N=10$ , and  $\Phi=0$ . Black indicates peak absorption, while white indicates peak gain; the intermediate scale is indicated in grey  $\times [8N(\pi eKL)^2 \rho / \gamma^3 mc^2]$ . Again, there is substantial gain off axis in several harmonics, but unlike the helical case, there is now gain on axis in the odd harmonics  $n=1, 3, 5, \dots$

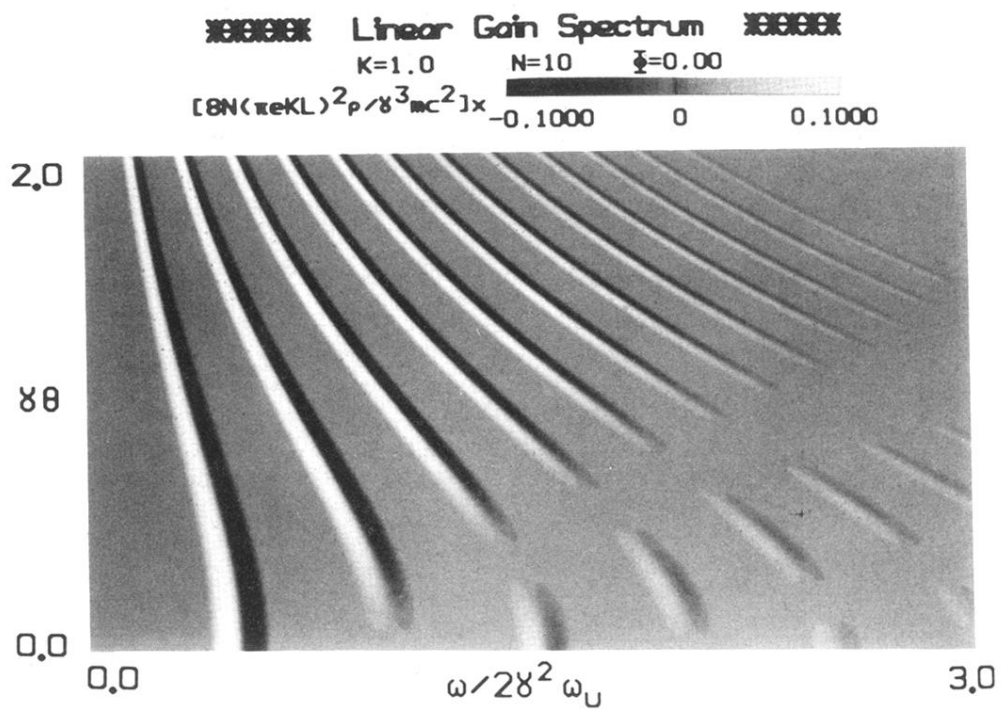


FIG. 12. FEL gain spectrum in a linear undulator is plotted for  $K=1.0$ ,  $N=10$ , and  $\Phi=0$ . At this higher value of  $K$ , there is much more gain available in the higher harmonics. The structure of the gain spectrum as a function of  $\vartheta$  can lead to some interesting effects when the optical wavefront is amplified.

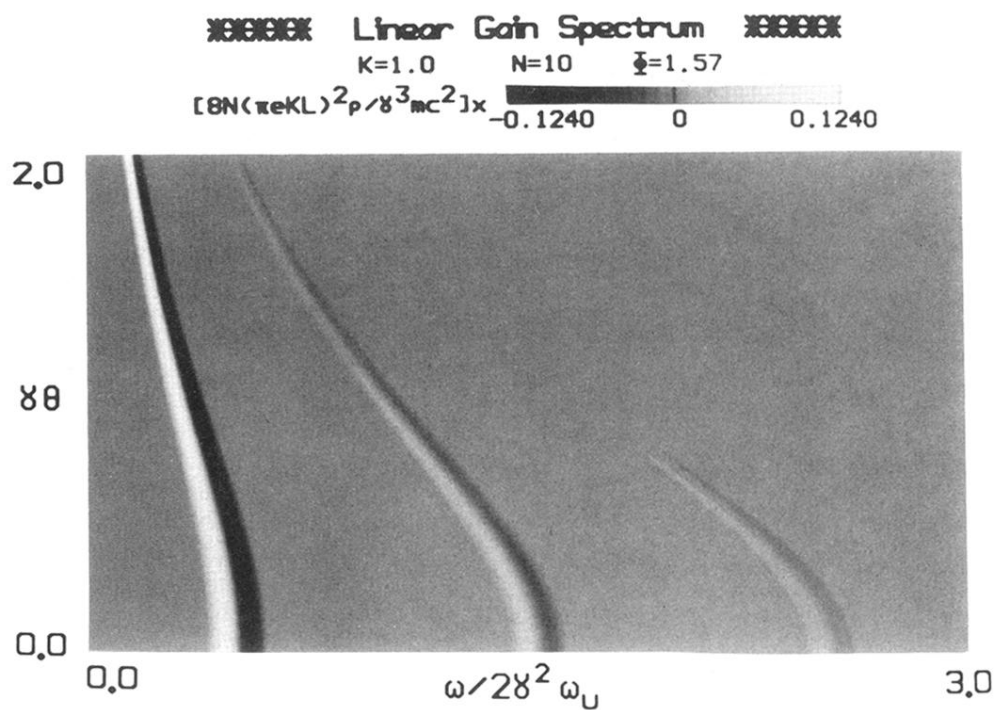


FIG. 13. FEL gain spectrum in a linear undulator is plotted for  $K = 1.0$ ,  $N = 10$ , and  $\Phi = \pi/2$ . At this observation angle, the gain in the even harmonics  $n = 2, 4, 6, \dots$  and the angular structure of the odd harmonics disappears.

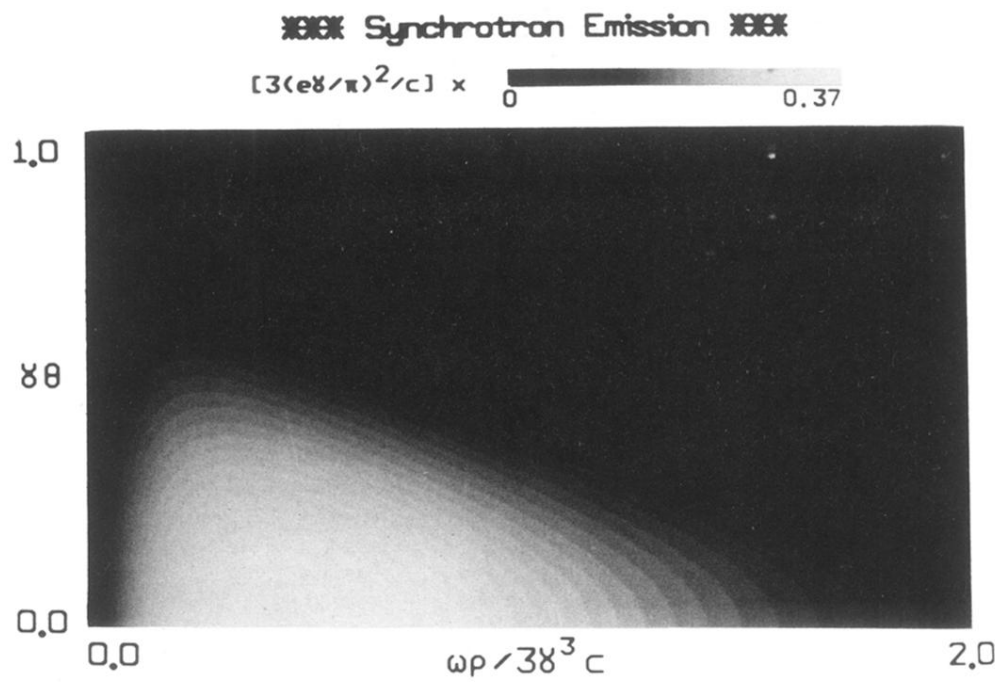


FIG. 14. Synchrotron spontaneous emission spectrum is plotted as a function of  $\gamma \vartheta$  and frequency  $\omega\rho/3\gamma^3c$  for an electron in a path of radius  $\rho$ . The intensity scale is indicated in grey  $\times [3(e\gamma/\pi)^2/c]$ . In contrast to the undulator cases, the synchrotron spectrum is broad in both frequency and angle. The characteristic angle is  $\vartheta \approx 0.5/\gamma$ , and the characteristic frequency is  $3\gamma^3c/\rho$ . While the total energy emitted is comparable to the undulators, the peak emission is less than an undulator by  $\times N^{-2}$ .

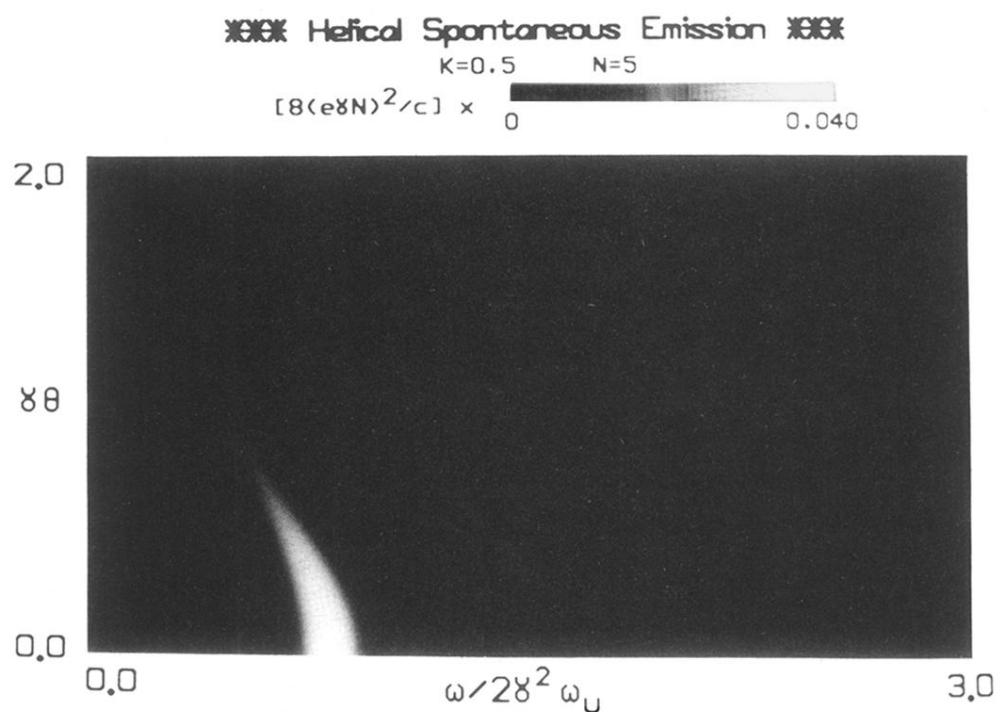


FIG. 2. FEL spontaneous emission intensity from a helical undulator is plotted as a function of  $\gamma\vartheta$  and frequency  $\omega/2\gamma^2\omega_u$  for  $K=0.5$  and  $N=5$ . The intensity scale is indicated in  $\text{grey} \times [8(e\gamma N)^2/c]$ . Only the fundamental shows emission at this small value of  $K$ .



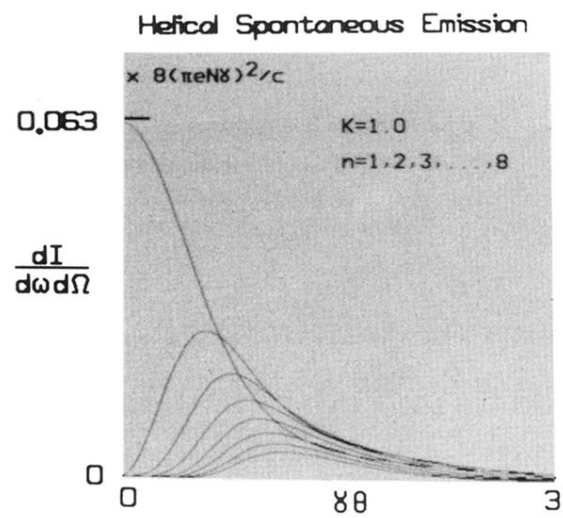


FIG. 4. The peak FEL spontaneous emission intensity from a helical undulator is plotted as a function of  $\gamma\vartheta$  in the first eight harmonics for  $K=1.0$ . Only the fundamental has emission on axis at  $\vartheta=0$ . As the harmonic number increases, the peak intensity decreases and moves to a larger value of  $\gamma\vartheta$ .

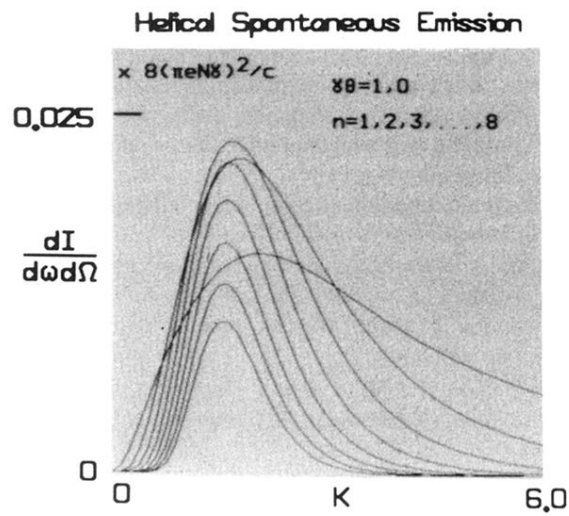


FIG. 5. The peak FEL spontaneous emission intensity from a helical undulator is plotted as a function of  $K$  in the first eight harmonics for  $\gamma\delta = 1.0$ . As the harmonic number increases, the peak intensity first increases, then decreases, and moves to smaller values of  $K$ . The fundamental,  $n = 1$ , is broader in  $K$ , while the higher harmonics are progressively more narrow.

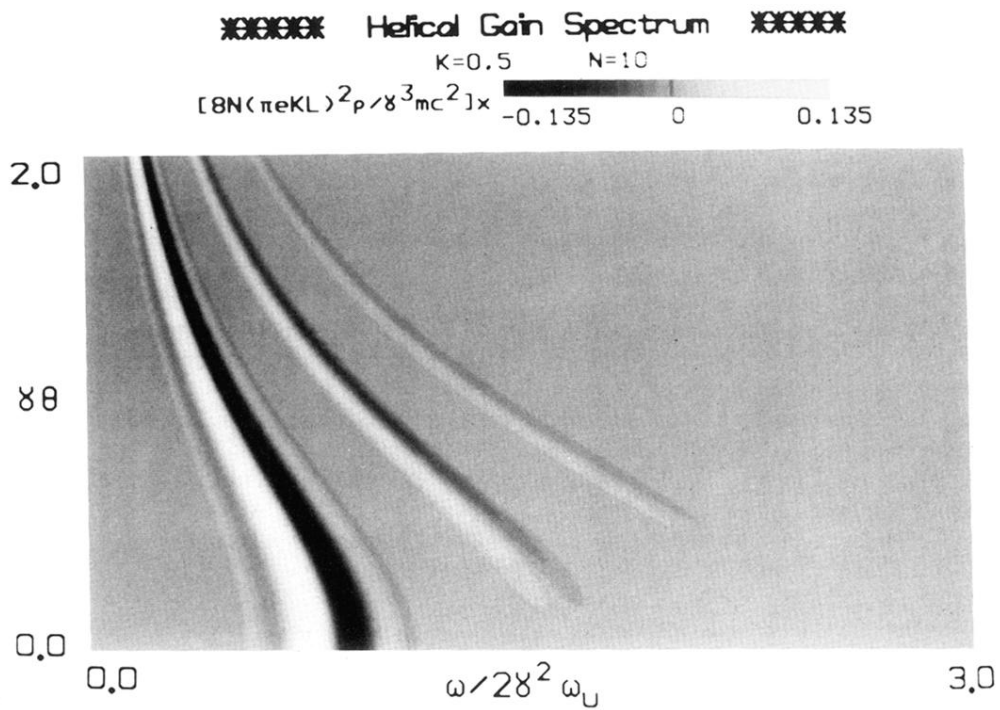


FIG. 6. FEL gain spectrum in a helical undulator is plotted for  $K=0.5$  and  $N=10$ . Black indicates peak absorption, or negative gain, while white indicates peak gain; the intermediate scale is indicated in grey  $\times [8N(\pi eKL)^2 \rho / \gamma^3 mc^2]$ . There is substantial gain off axis and the frequency  $\omega$  can be tuned over a large range with almost no decrease in coupling. At this low value of  $K$ , the gain in higher harmonics is much less than in the fundamental. There is no gain on axis except at the fundamental.

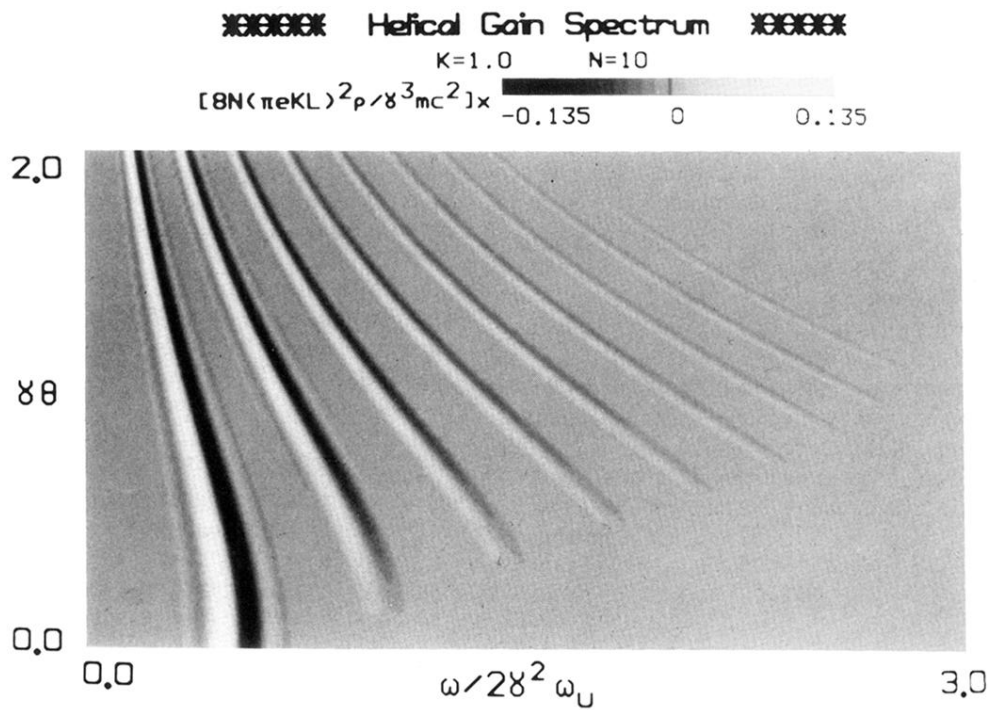


FIG. 7. FEL gain spectrum in a helical undulator is plotted for  $K = 1.0$  and  $N = 10$ . Again there is substantial gain off axis, but with this increased value of  $K$ , the gain in higher harmonics is now comparable to the gain in the fundamental. Comparison with Fig. 3 shows gain only occurs where there is spontaneous emission, since each process must roughly satisfy the resonance condition  $\nu_n \approx 0$ . As the optical resonator is tilted in angle  $\vartheta$ , the FEL can be tuned to a large range of frequencies with good coupling.

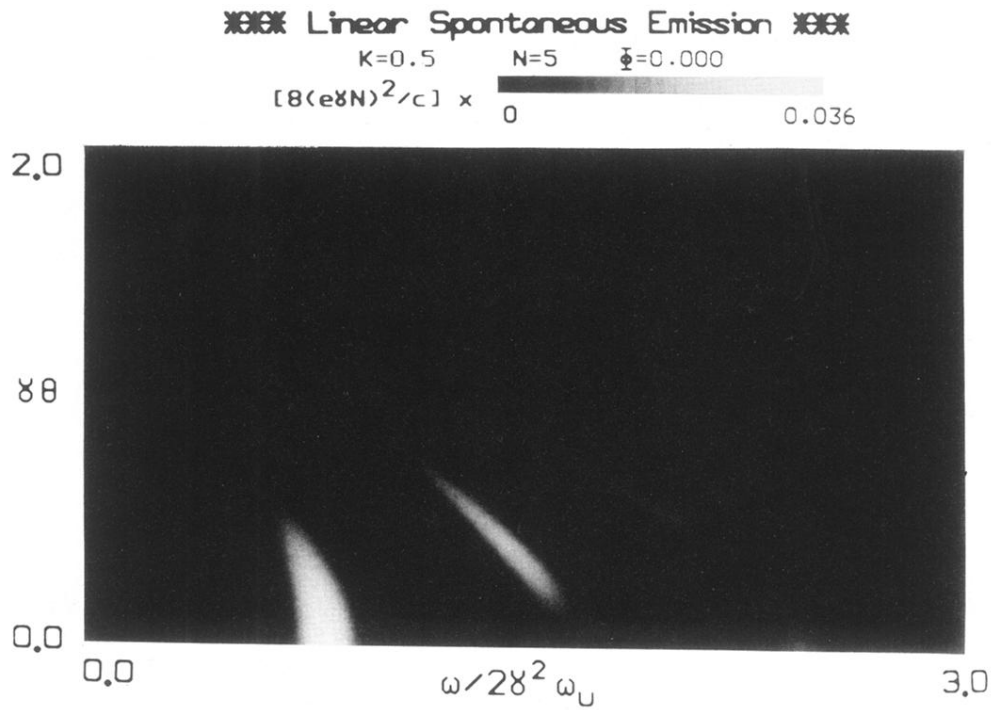


FIG. 8. FEL spontaneous emission intensity from a linear undulator is plotted for  $K=0.5$ ,  $N=5$ , and observed at  $\Phi=0$ . The intensity scale is indicated in grey  $\times [8(e\gamma N)^2/c]$ . In addition to emission at the fundamental, there is emission in the first harmonic off axis.

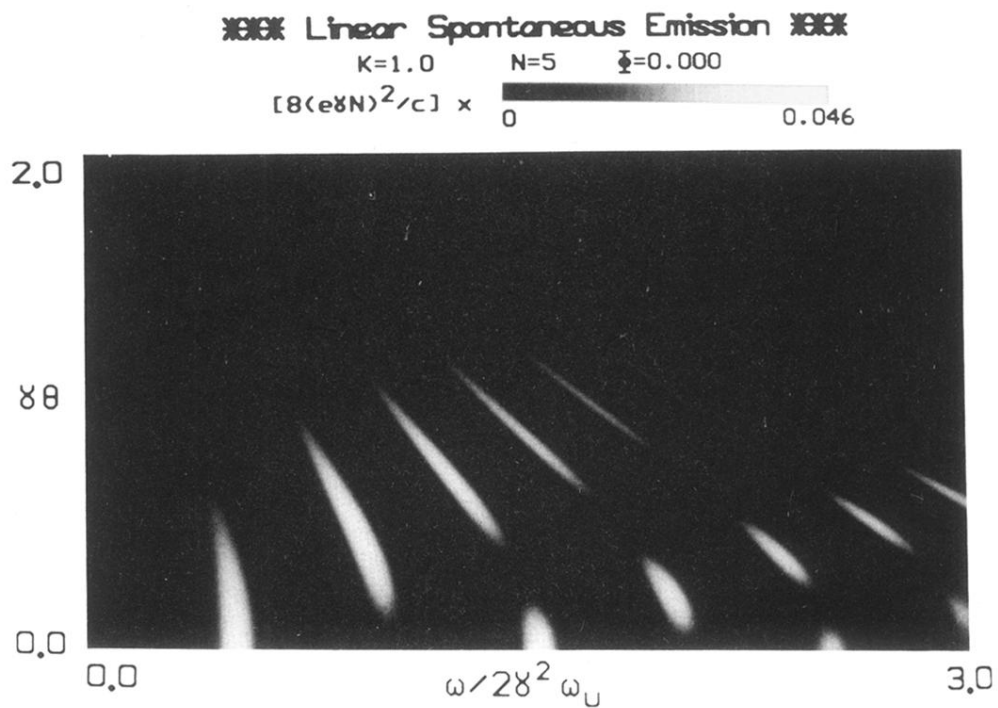


FIG. 9. FEL spontaneous emission intensity from a linear undulator is plotted for  $K = 1.0$ ,  $N = 5$ , and observed at  $\Phi = 0$ . At this higher value of  $K$ , there is increased emission in several higher harmonics. Unlike the helical undulator case, the linear case has emission on axis in the odd harmonics  $n = 1, 3, 5, \dots$ . In all harmonics, there is structure in the angle  $\vartheta$ , which gives a more complicated spectrum. This is because the motion in a linear undulator is more complicated than in the helical case.